Detailed experimental and computation/molecular simulation of 1,5-benzodiazepin derivative as corrosion inhibitor for E24 steel in 1 M HCl environment

S. Ksama,[1] K. Tassaoui,[1] A. Chraka,[2] K. Chkirate,[3] M. Damej,[1] N. Ouadghiri,[3] M. Errili,[1] K. Azgaou,[4] E.M. Essassi,[3] H.T. Rahal[5] and M. Benmessaoud[1]*

[1]Energy, Materials and Sustainable Development Team CERNE2D, Higher School of Technology Salé, Mohammed V University in Rabat 8007, Morocco
[2]Laboratory of Materials Engineering and Sustainable Energy (IMED-LAB), Faculty of Science, Abdelmalek Essaadi University, Tetouan, Morocco
[3]Laboratory of Heterocyclic Organic Chemistry URAC 21, Pharmacochemistry Competence Center, Av. Ibn Battouta, BP 1014, Faculty of Sciences, Mohammed V University in Rabat, 10010, Rabat, Morocco
[4]Laboratoire S3MN2E-CERNE2D, Faculty of Sciences, Mohammed V University in Rabat, Av. Ibn Battouta, B.P. 1014, M10000 Rabat, Morocco
[5]Department of Chemistry, Faculty of Science, Lebanese International University, Lebanon
**E-mail: mohammed.benmessaoud@est.um5.ac.ma*

Abstract

A novel synthetic chemical, namely (*Z*)-7-methyl-4-(2-oxopropylidene)-[1,5]-benzodiazepin-2-one (BZ-Me), was characterized using ^{1}H NMR and ^{13}C NMR techniques. Its ability to minimize the corrosion of E24 steel in a 1 M hydrochloric acid solution was experimentally evaluated using various techniques, including stationary electrochemical techniques (PDP), electrochemical impedance spectroscopy (EIS), density functional theory (DFT) methods, and Monte Carlo (MC) simulations. Combining EDX assessment with scanning electron microscopy (SEM) allowed for an investigation of the surface morphology of E24 steel both alone and in the presence of the inhibitor. Both approaches are in excellent agreement, indicating that the BZ-Me compound functions as a mixed inhibitor with a maximum effectiveness of 90% (according to the polarization curve) and 88% (according to the EIS methodology) for a concentration of 1 mM. In addition, the charge transfer resistance rises as inhibitor concentrations and immersion durations increase, as seen in the electrochemical impedance spectrum. Conversely, the interfacial capacitance decreases with higher inhibitor concentrations and longer immersion durations. Based on Langmuir's isotherm, the tests have demonstrated that BZ-Me attaches to the E24 steel surface with a standard free energy $|\Delta G^{0}_{ads}|$ of 36.17 kJ·mol^{-1}. This indicates that BZ-Me uses both physical and chemical adsorption to prevent the corrosion process. The surface morphological observation revealed that BZ-Me forms a barrier of protection that inhibits the transfer of active corrosive species to E24 steel surfaces, compared

to the blank test. Furthermore, the offered theoretical results confirmed the experimental results obtained.

Received: May 20, 2024. Published: October 21, 2024 doi: 10.17675/2305-6894-2024-13-4-9

Keywords: *corrosion, inhibition, E24 steel, Tafel measurements, benzodiazepine derivative, SEM/EDX, DFT.*

1. Introduction

Sustainable materials have been extensively utilized in various applications that reduce the pollution caused by chemicals and their use [1]. Several industrial facilities frequently use iron and iron-based alloys of various grades as construction materials, which include acids, alkalis, and salt solutions, due to their inexpensive price and exceptional strength [2]. Most research activities in recent years have concentrated on producing environmentally friendly and cost-effective inhibitors. As a general rule, organic inhibitors work to minimize metal corrosion by forming a barrier of protection on the metal surface through either chemisorption or physisorption. To mitigate the undesirable rate of metal dissolution, a common and effective method involves adding small quantities of both organic and inorganic chemicals to the corrosive environment [3, 4]. In particular, compounds with heteroatoms or multiple bonds serve as effective corrosion inhibitors and adsorption centers because they contain lone pairs. Nanomaterials are more useful because of interactions between functional groups and the metal surface. These interactions include loading, surface activity, and polymerization [5]. The group of chemical compounds known as benzodiazepines is crucial to both pharmacological and biological research. Owing to their wide variety of applications, their derivatives have attracted significant interest in the domains of medicinal chemistry [6–8]. Most people use them as medications to treat anxiety, panic attacks, agitation, sleeplessness, and amnesia. They do not appear to be especially dangerous to the environment. Furthermore, they are economical and easy to prepare [9–11]. Typically, the synthesis of 1,5-benzodiazepines involves the combination of *o*-phenylenediamine with α,β-unsaturated carbonyl compounds, β-haloketones, or ketones in acidic environments. These acidic conditions play a crucial role in enhancing the condensation process [12]. In the limited research on their use as corrosion inhibitors, according to El Ibrahimi [13], three derivatives of 1,5-benzodiazepin-2-one (DMBD: 4,7-dimethyl-1,5-benzodiazepin-2-one, PBD: 3-phenyl-1,5-benzodiazepin-2-one, and MPBD: 4-methyl-7-phenyl-1,5-benzodiazepin-2-one) prevented iron from dissolving in an acidic environment. In another study, Sebhaoui *et al*. [14] stated 4-(2-oxopropylidene)-1-propargyl-1,2,4,5-tetrahydro-3*H*-1,5-benzodiazepin-2-one (PTB) and 1-decyl-4-(2-oxopropylidene)-1,2,4,5-tetrahydro-3*H*-1,5-benzodiazepine-2-one (DTB) as two efficient substances that prevent carbon steel from corroding in a solution of 1 M HCl. Moreover, Laabaissi *et al*. [15] discovered that mild steel may effectively be protected against corrosion

in an acidic environment by the benzodiazepine derivative. To our knowledge, only a limited number of studies have explored the use of benzodiazepines as corrosion inhibitors. Inspired by these findings, the investigation was continued by our team, leading to the development of new compounds and the exploration of their inhibitory potential. In this context, the present study was conducted to establish a correlation between previously reported inhibition efficiencies and the specific structural characteristics of a new benzodiazepine compound, namely (*Z*)-7-methyl-4-(2-oxopropylidene)-[1,5]-benzodiazepin-2-one (BZ-Me). The inhibition mechanism for corrosion on E24 steel in a 1 M HCl solution was thoroughly investigated using traditional methods, including potentiodynamic polarization (PDP) and electrochemical impedance spectroscopy (EIS) tests. Additionally, the adsorption isotherm of the inhibitor on the E24 steel surface was determined, along with the standard free energy of adsorption (ΔG_{ads}). The influence of immersion time in the corrosive solution was also examined, and the surface morphology was analyzed. To further understand the corrosion inhibition process, the tested inhibitor was subjected to molecular-level analysis through computational methods and molecular simulation.

2. Materials and Methods

2.1. Synthesis of inhibitor

Figure 1 presents the synthesis procedure of (*Z*)-7-methyl-4-(2-oxopropylidene)-4,5-dihydro-1*H*-[1,5]-benzodiazepin-2(3*H*)-one (BZ-Me). The derivative was prepared by the reaction of a solution of dehydroacetic acid 2 (3.36 g, 0.02 mol) and 4-methyl-*o*-phenylenediamine 1 (4.32 g, 0.04 mol) in xylene (80 mL) and refluxed for 4 h. Next, the precipitated product was filtered under reduced pressure and then recrystallized with ethanol. The resulting product underwent characterization *via* ^{1}H NMR, ^{13}C NMR, and Heteronuclear 2D (Figures 2, 3, and 4).

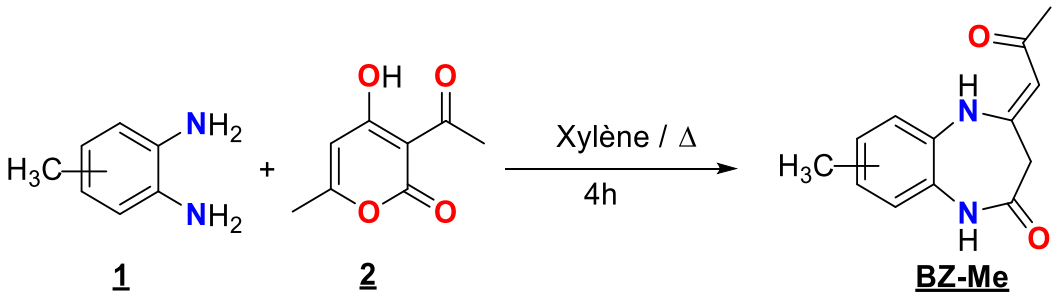

Figure 1. Procedure for the synthesis of (*Z*)-7-methyl-4-(2-oxopropylidene)-4,5-dihydro-1*H*-[1,5]-benzodiazepin-2(3*H*)-one (BZ-Me).

(*Z*)-7-Methyl-4-(2-oxopropylidene)-4,5-dihydro-1*H*-[1,5]-benzodiazepin-2(3*H*)-one (referred to as compound BZ-Me) was obtained as a yellow solid with a melting point of 242–244°C (in ethanol). Its thin-layer chromatography (TLC) profile, using a mixture of

cyclohexane and ethyl acetate (8/2, v/v), displayed a Rf value of 0.15. The compound's proton nuclear magnetic resonance (^{1}H NMR) spectrum, recorded at 300 MHz in DMSO-d_6, revealed the following chemical shifts (δ in ppm): 2.04–2.27 (two singlets, 2CH_3); 3.10 (singlet, 2H, CH_2); 5.31 (singlet, 1H, CH_{vinyle}); 6.92–7.13 (multiplet, 3H, CH_{ar}); 10.29 (singlet, 1H, NH); 12.32 (singlet, 1H, NH). The compound's carbon-13 nuclear magnetic resonance (^{13}C NMR) spectrum, recorded at 75 MHz in DMSO-d_6, displayed the following chemical shifts (δ in ppm): 20.80 (CH_3); 29.49 (CH_3); 41.63 (CH_2); 95.88 (CH_{vinyl}); 123.02–126.24 (CH_{ar}); 128.51–168.14 (C_q).

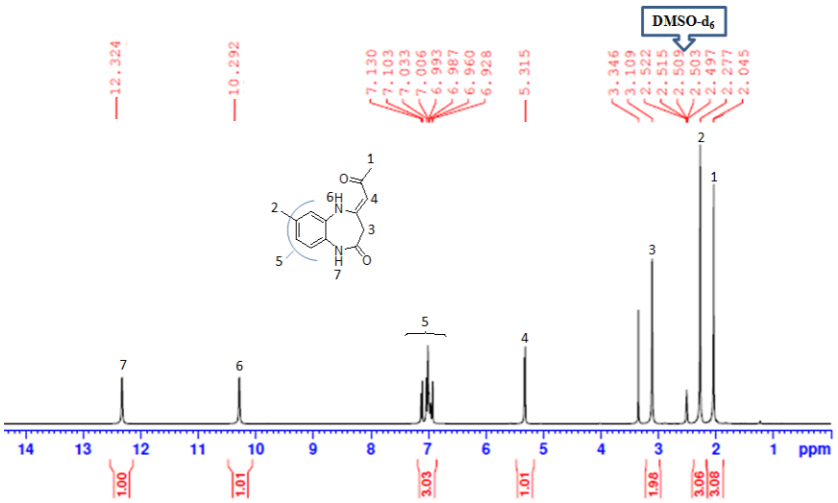

Figure 2. ^{1}H NMR spectrum of (BZ-Me).

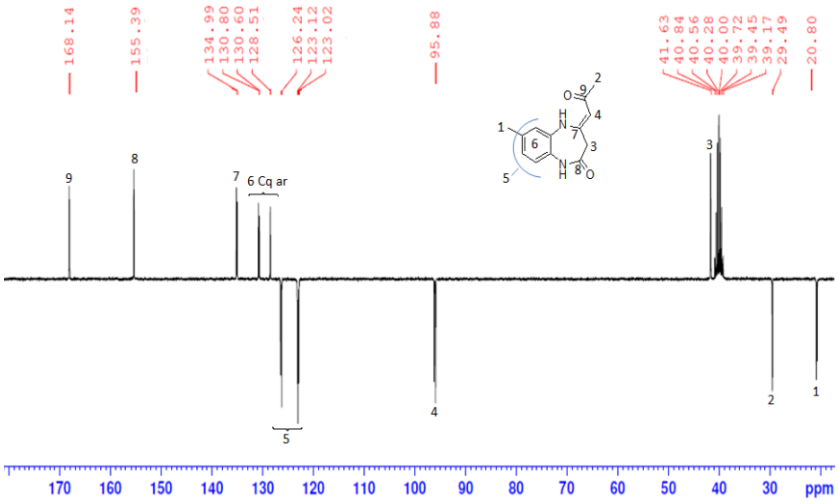

Figure 3. ^{13}C NMR spectrum of (BZ-Me).

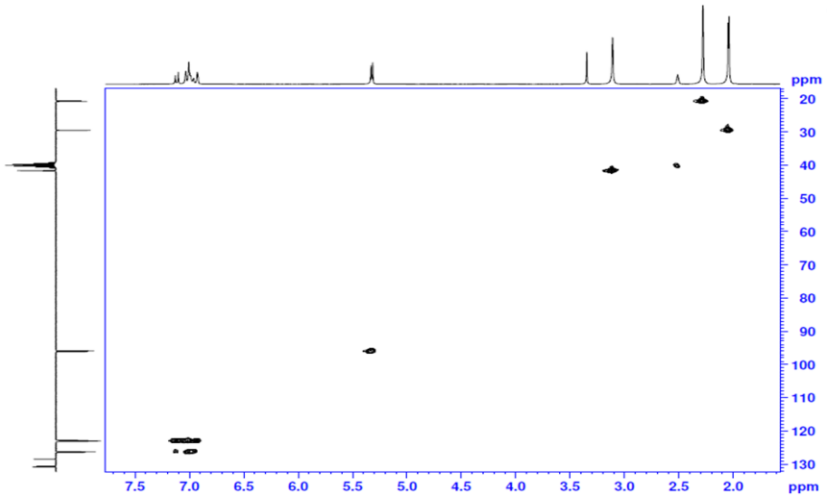

Figure 4. Heteronuclear 2D spectrum of (BZ-Me).

2.2. Electrodes, test solution

The electrochemical measurements were conducted using rectangular samples of carbon steel (E24) with an area of 0.785 cm^2. The remaining portion of the mild steel electrode was coated with epoxy resin for insulation, and the specified chemical composition was: Mn=0.52%, Si=0.24%, C=0.11%, Cr=0.12%, Ni=0.10%, Cu=0.14% and the remainder Fe. Before conducting any studies, all specimens were sequentially polished using emery paper of grades 400, 600, 1000, 1500, and 2000. After that, they were cleaned with distilled water, treated with acetone to remove oil, let air dry, and allowed to dry at room temperature. As for the aggressive medium of 1 M HCl involved in all the tests, was prepared *via* diluting of analytical reagent-grade 37% HCl with distilled water.

2.3. Electrochemical measurements

The electrochemical examinations were conducted methodically employing a VoltaLab-PGZ-100, which is managed by the control of the Volta Master 4 analyzing software. A common three-electrode cell system is fitted with a working electrode (E24 steel), a reference electrode (Ag/AgCl/KCl), and an auxiliary electrode (platinum rod). The saturated calomel electrode (*vs.* SCE) served as the standard for all potentials. Before assessing the electrochemical performance of the E24 steel in corrosive solution, the working electrode was left in the test solution for over 60 minutes at a temperature of 298 K to maintain the open circuit potential (OCP) voltage. The polarization readings were outlined over a scale of –800 to –100 mV/ECS, with an automatic scan rate of 1 mV/s. Meanwhile, alternating current (AC) signals with a peak-to-peak amplitude of 10 mV were used for electrochemical impedance spectroscopy (EIS) investigations. The measurements were performed through the frequency range of 100 kHz to 10 mHz under varied situations. The data acquired from both the PDP and EIS approaches were assessed and manipulated utilizing graphing and impedance analysis programs, namely EC-Lab.

2.4. Surface morphology

The morphological and elemental composition of the E24 steel, both without or with 1 mM of BZ-Me in 1 M HCl solution, were analyzed through a thermo-scientific Quattro S scanning electron microscope (SEM) incorporating energy-dispersive X-ray spectroscopy (EDX). The surface morphological structure, average roughness, and hydrophobicity of E24 surfaces were assessed after immersing them for 24 hours. We conducted the research at the Laboratory SEM/EDX, one of the Technical Support Units for Scientific Research affiliated with the National Center for Scientific and Technical Research.

2.5. Computational details

2.5.1. Ab initio DFT modeling

The Initio Density Functional Theory (DFT) method [16, 17] was used in this work to predict the structural and global reactivity of the neutral form of BZ-Me. Optimizing the geometrical structure of the title molecule was done by PBEPBE level at 6-31+G(d,p) basis set [18, 19]. All Ab-initio DFT calculations were performed using the Gaussian 09 program package. The DFT study has been used for analyses of Frontier Molecular Orbitals (FMOs), molecular electrostatic potentials (MEP), contour representation of ESP distributions, Mulliken charge distribution [20], and electronic descriptors including the energies of highest occupied, lowest unoccupied molecular orbital (E_{HOMO} and E_{LUMO}), the frontier orbital energy gap (ΔE_{gap}), the electron affinity (*EA*), the ionization potential (*IP*), the electronegativity (χ), the chemical hardness (η), the softness (*S*), electron-accepting power (ω^+), electron-donating power (ω^-), back-donation ($\Delta_{back\text{-}donation}$), the fraction of electrons transferred (ΔN), and metal/inhibitor interaction energy ($\Delta\psi$) were calculated according to Equations (1–11) as reported in the literature [21]:

$$IP = -E_{HOMO} \tag{1}$$

$$EA = -E_{LUMO} \tag{2}$$

$$\Delta E_{gap} = E_{LUMO} - E_{HOMO} \tag{3}$$

$$\chi = \frac{IP + EA}{2} \tag{4}$$

$$\eta = \frac{IP - EA}{2} \tag{5}$$

$$S = \frac{1}{\eta} \tag{6}$$

$$\omega^+ = \frac{(IP + 3EA)^2}{16(IP - EA)} \tag{7}$$

$$\omega^- = \frac{(3IP + EA)^2}{16(IP - EA)} \tag{8}$$

$$\Delta_{\text{back-donation}} = -\frac{\eta}{4} \tag{9}$$

$$\Delta N = \frac{\varphi_{\text{Fe}} - \chi_{\text{inhibitor}}}{2(\eta_{\text{Fe}} + \eta_{\text{inhibitor}})} \tag{10}$$

$$\Delta \psi = \frac{\varphi_{\text{Fe}} - \chi^2_{\text{inhibitor}}}{4(\eta_{\text{Fe}} + \eta_{\text{inhibitor}})} \tag{11}$$

where η_{Fe} represents the absolute hardness of iron, with a value of 0 eV·mol^{-1} and χ_{Fe} is the work function (4.81 eV·mol^{-1}) of the Fe surface (Fe (110)).To further study the local reactivity of BZ-Me, we performed a detailed analysis using DFT, focusing on molecular electrostatic potentials (MEP), Mulliken charges, and electrostatic potential (ESP) distributions. This approach allowed us to gain deeper insights into the molecular interactions and potential reaction sites of BZ-Me.

2.5.2. Simulation details

To study the nature of the interaction between the BZ-Me onto Fe-substrate, we used the molecular dynamics (MD) simulations [22, 23] implemented using the Material Studio 8.0 software from the BIOVIA company. According to earlier reports for the representation of carbon steel, Fe (110) surface was adopted [24, 25]. The interactions BZ-Me–iron (Fe) substrate in the simulated corrosion media performed *via* the Fe (110) supercell of size (12×12) and a vacuum slab with (50 Å) thickness in a simulation box (32 Å×32 Å×6 Å) [26]. The potential energy values required for molecular interactions were derived from the COMPASSII force field during MD simulations [27] This force field, which successfully predicts various gas-condensed-phase properties of a variety of compounds, has previously been used in investigations of inorganic and organic systems [28–30]. Furthermore, MD was achieved using an NVT canonical ensemble at 293 K, 1 fs time step, and 400 picoseconds simulation period.

3. Results and Discussion

3.1. Open circuit potential

The open circuit potential refers to the electrical potential difference between the reference electrode and the working electrode when no current is flowing through the circuit. It was used to record the polarization and impedance of inhibitors in a corrosive environment to reach a quasi-stationary state [31]. Additionally, studying the OCP shifts over time of the working electrode is crucial for identifying corrosion zones, complete and partial inhibition, and inhibitor-threshold concentrations [32]. Figure 5 presents the plot of OCP time plots for E24 steel in the uninhibited and inhibited BZ-Me solutions in 1 M HCl at 293 K. In an uninhibited test, (E_{corr} at t=3600 s) values in the steady state are consistently higher than the immersion potential (E_{OCP} at t=0). After a few minutes, the metal reached a stable condition, which is consistent with free corrosion [33]. In contrast, adding BZ-Me to the corrosive

solution shifts the potential value into the positive region at all studied concentrations. Furthermore, the potential progressively becomes stable after a certain period, both with and without the presence of BZ-Me, as has been observed in several experiments [34–36].

3.2. Potentiodynamic polarization (PDP)

Potentiodynamic anodic and cathodic polarization graphs for E24 steel in an acidic medium with and without diverse amounts of BZ-Me at 293 K are displayed in Figure 6. The electrochemical parameters, comprising corrosion current density (i_{corr}), corrosion potential (E_{corr}), cathodic and anodic Tafel slopes (b_c and b_a), and inhibition efficiency (*IE*%) are determined and listed in Table 1. The inhibition efficiency of polarization curves was determined with the following Equation (12) [37]:

$$IE\% = \frac{i^0_{corr} - i_{corr}}{i^0_{corr}} \quad (12)$$

where i^0_{corr} and i_{corr} are the corrosion current density values in the absence and presence of BZ-Me, respectively, ascertained by extrapolation of the Tafel lines to the corrosion potential.

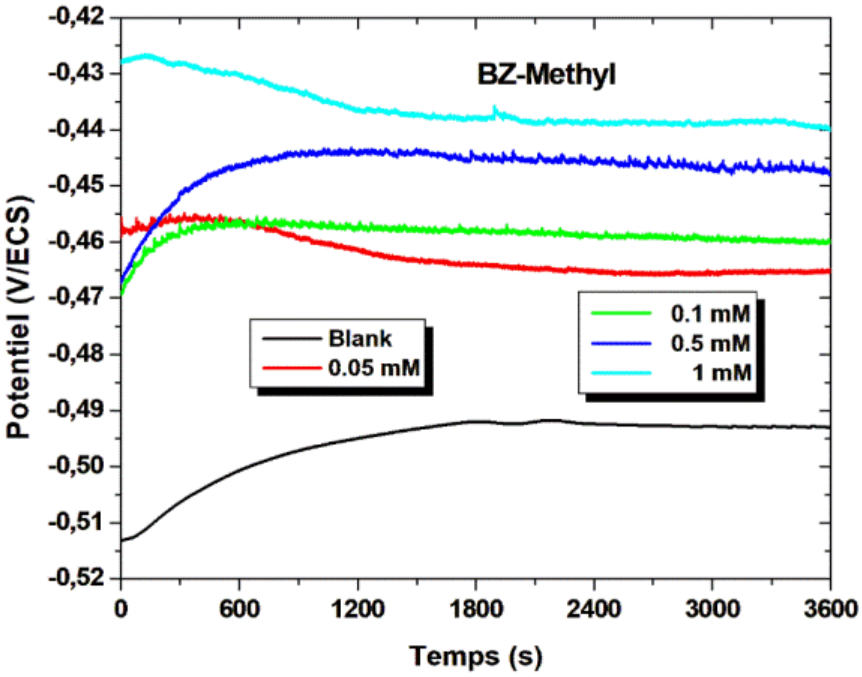

Figure 5. Open circuit potential *vs.* time for E24 steel alone and with BZ-Me at different amounts in 1 M HCl solution at 293 K.

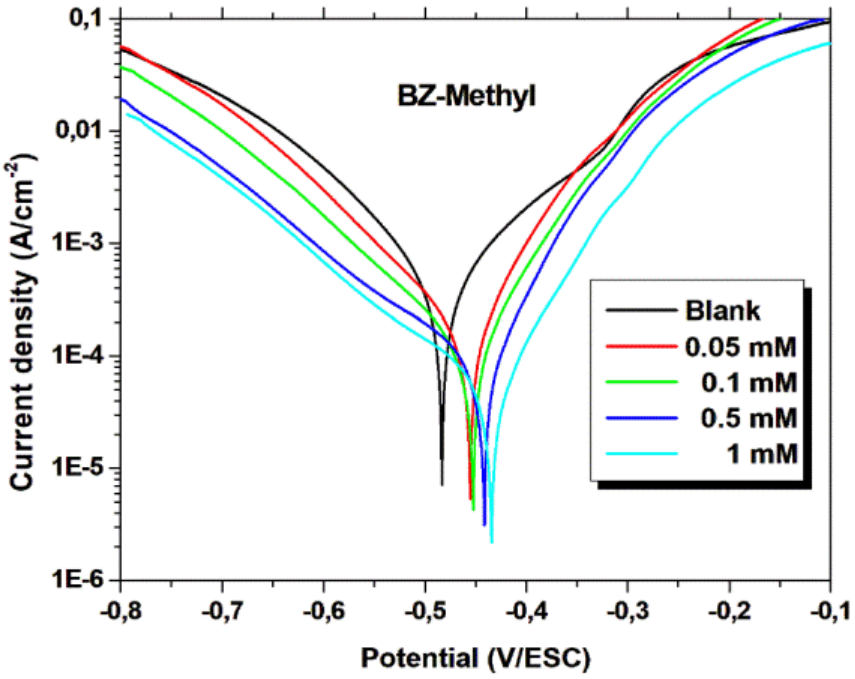

Figure 6. PDP plots for E24 steel alone and with BZ-Me at different amounts in 1 M HCl solution at 293 K.

Based on the preliminary study of this diagram (Figure 6), the introduction of BZ-Me to the corrosive solution lowers the cathodic and anodic curve slopes, which results in a significant reduction in the rate of oxidation of the metal at the anode and the reduction of H^+ ions at the cathode at all measured concentrations [38]. While there is a shift in E_{corr} values towards positive values for BZ-Me compared to the blank test, which aligns with what is reported in the literature [39–41], if the absolute difference in corrosion potential (E_{corr}) between the inhibitory and uninhibited solutions is under 85 mV, then the inhibitors may be categorized as mixed types. Since the observed change equals 49 mV *vs*. SCE, it suggests that BZ-Me may be categorized as a mixed type with a major anodic effectiveness [42]. However, the data presented in Table 1 reveal a little shift in the values of b_a and b_c after adding BZ-Me, this variation suggests that the inhibitor molecules do not significantly affect the mechanism of E24 dissolution and hydrogen formation processes [43]. Instead, it reduces the occurrence of both reactions and adsorbed onto the metal surface by inhibiting the active sites on the metal/solution interface, hence reducing the corrosion reaction. In addition, the level of inhibitory effectiveness rises as the concentrations of BZ-Me increase, ultimately reaching a peak value of 90.78% at a concentration of 1 mM, which demonstrates that BZ-Me behaves like an extremely efficient inhibitor for preventing the corrosion of E24 steel in HCl environment. Additionally, the presence of nitrogen and oxygen atoms in the BZ-Me plays a significant function as adsorption sites and contributes to molecular interactions with E24 steel. This is likely responsible for the compound's inhibitory activity [44].

Table 1. The values of the descriptor potentiodynamic parameters for E24 steel alone and with BZ-Me at different amounts in 1 M HCl solution at 293 K.

[BZ-Methyl] (mM)	E_{corr} (mV/Ag–AgCl)	i_{corr} (μA/cm^2)	b_a (mV/dec)	b_c (mV/dec)	*IE*%
0	–483	340.6	–94.2	91.3	
0.05	–455	101.3	–89.7	58.9	70.27
0.1	–452	77.1	–91.3	62.1	77.36
0.5	–441	53.3	–120.1	54.6	84.35
1	–434	31.4	–115.6	60.6	90.78

3.3. Electrochemical impedance spectroscopy (EIS)

3.3.1. Concentration effect

In corrosion research, electrochemical impedance spectroscopy (EIS) is recognized and powerful. It provides information on surface qualities, electrode kinetics, and mechanisms [45, 46]. Figures 7 and 8 depict the Nyquist, Bode, and Phase plots to evaluate the corrosion resistance of E24 steel in an acidic environment alone and with different concentrations of BZ-Me at 293 K. The Nyquist plot (Figure 7) exhibits a large single capacitive loop, which is clearly defined as a time constant in the Bode plot (Figure 8). According to this discovery, charge transfer activities dominated the corrosion process [47], and the inhibitor forms a highly effective interface barrier that inhibits the E24 steel surface [48]. The overall assessment results show that it expands as the concentration of BZ-Me rises. It implies that the inhibition efficiency is related to the concentration of the inhibitor tested. Significantly, the rough and heterogeneous surface of the electrode contributes to the frequency dispersion, as seen by the imperfect semicircles illustrated in Figure 7 [49–52]. Besides, the data suggest that the inhibitor raises the value of R_{ct}, and the following Equation (13) measures the inhibition efficiency [53]:

$$IE\% = \frac{R_{ct}^{i} - R_{ct}^{0}}{R_{ct}^{i}} \cdot 100\% \tag{13}$$

Furthermore, a higher concentration of BZ-Me causes the samples to exhibit increased impedance at low frequencies, according to the Bode (module/phase) plots indicated in Figure 8. It is worth noting that the BZ-Me molecules stick at the surface of the sample, forming a protective layer that inhibits metal corrosion. Furthermore, the phase angle of the sample impedances is approximately 65° at high frequencies, indicating that the impedance represents an impure capacitance [25].

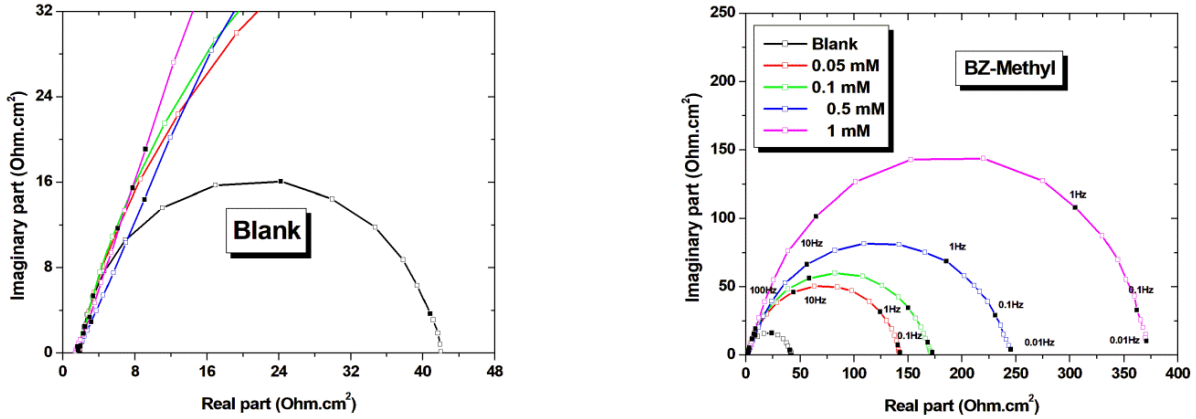

Figure 7. Nyquist curve of E24 steel alone and with BZ-Me at different amounts in 1 M HCl solution at 293 K.

To get a more profound comprehension of the characteristics of the interface between the electrode and the solution, an electrical equivalent circuit was proposed (Figure 9), this circuit closely matches the impedance data presented in Figure 7 and is detailed in Table 2. The system is composed of three components: R_s (the solution resistance), R_{ct} (the charge transfer resistance), and CPE_{dl}, (the interfacial capacitance instead of a pure capacitor). Although the Nyquist plots reveal a depressed capacitive loop, the relationship between the double-layer capacitance (C_{dl}) and the constant phase element (CPE_{dl}) is expressed by the given Equation (14) [54]:

$$C_{dl} = Y_0 \omega^{n-1} = Y_0 (2\pi f)^{n-1} \tag{14}$$

where Y_0 is the admittance, n represents the exponent of the CPE ($-1 \leq n \leq 1$), ω is the angular frequency, and the fitted variables are provided in detail in Table 3.

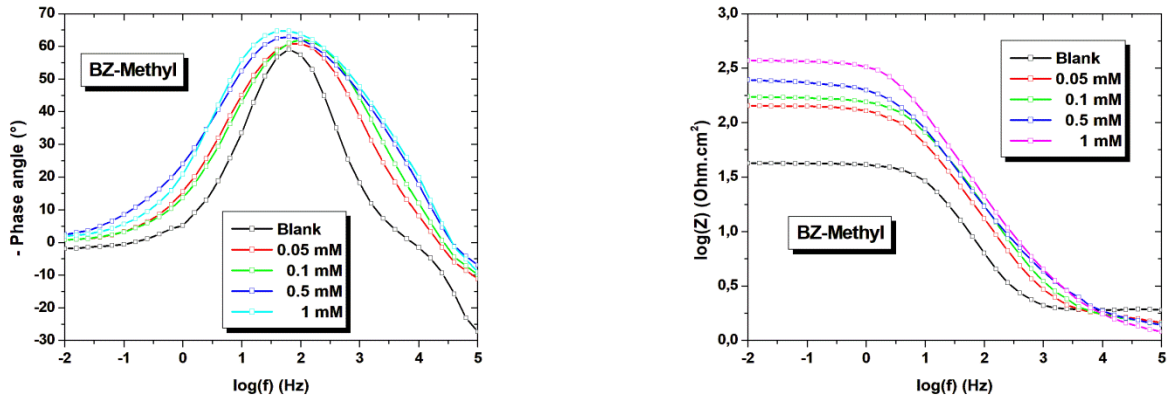

Figure 8. Bode modulus and Phase Angle curves of E24 steel alone and with BZ-Me at different amounts in 1 M HCl solution at 293 K.

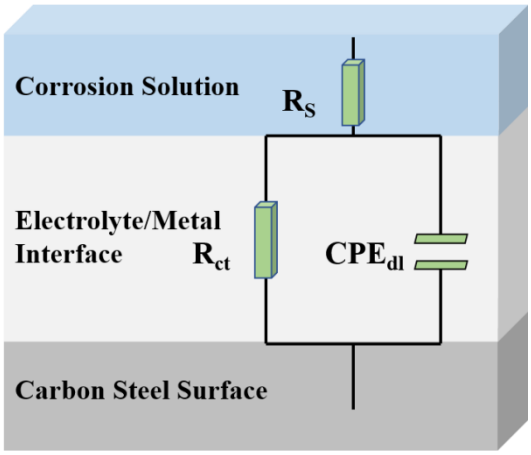

Figure 9. Electric equivalent circuit.

Table 2. The values of the descriptor electrochemical impedance parameters for E24 steel alone and with BZ-Me at different amounts in 1 M HCl solution at 293 K.

[BZ-Me] (mM)	R_s (Ω·cm^2)	R_{ct} (Ω·cm^2)	CPE_{dl} (μF·cm^{-2})	*n*	*IE* (%)	θ
0	1.76	42.63	589.9	0.84	–	–
0.05	1.73	139.7	113.9	0.82	69.49	0.6949
0.1	1.47	170.1	93.6	0.81	74.94	0.7494
0.5	1.42	241.7	65.9	0.75	82.36	0.8236
1	1.28	372.3	42.8	0.76	88.55	0.8855

According to Table 2, a lower n value about increased quantities confirms the increase in the heterogeneous surface. Additionally, the selection values of inhibitor concentration raise the R_{ct} progressively and reduce the CPE_{dl} bit by bit. This indicates that the protective layer becomes thicker, which works as a barrier against E24 substrate corrosion. The highest level of inhibition efficiency was achieved at 88.85% at 1 mM of BZ-Me, which is compatible with the data obtained from the Tafel experiment. Furthermore, the efficiency can be evaluated using:

$$IE\% = \frac{CPE_{dl}^{0} - CPE_{dl}^{i}}{CPE_{dl}^{0}} \cdot 100\% \quad (15)$$

The obtained values are slightly higher than those obtained by transfer resistance and close to the polarization data. These findings agree the explanation introduced by Cao, 1996, that when the E_{corr} is not affected by the presence of the inhibitor as well as Tafel slopes, the inhibitor acted *via* a geometric blockage at the metal surface could be clarified for better readability and accuracy [55, 56].

3.3.2. Immersion effect

To better understand the consequences of immersion time on the corrosion properties and the adsorption phenomenon of E24 steel in 1 M HCl medium, an electrochemical impedance spectroscopy test was conducted. Figures 10 and 11 illustrate the Nyquist, Bode, and Phase illustrations at the corrosion potential for a 1 mM concentration of BZ-Me. These graphs depict a distinct semicircle over time [57–59]. Table 3 compiles the electrochemical variables extracted from the EIS curves. As the amount of immersion time increases, the electrochemical impedance plots maintain their original shape, but the diameter of the semicircle in the Nyquist plot (Figure 10) sharply increases. At the same time, the $|Z|$ *vs.* frequency plot (Figure 11) shows that the phase angle of the BZ-Me rises as the immersion time increases and shifts towards a higher frequency, reaching close to 70° after 24 h, indicating that it is a pure capacitance impedance [60]. Based on these results, it appears that BZ-Me's ability to stop corrosion is because it creates a very strong barrier around the surface of E24 steel. This layer stops the corrosion process from occurring.

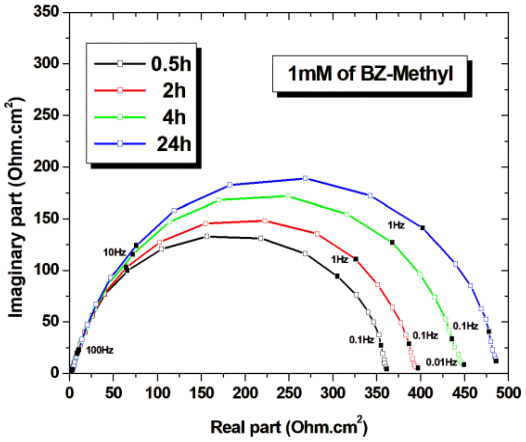

Figure 10. Nyquist plot of E24 steel at different immersion times in 1 M HCl solution at 293 K.

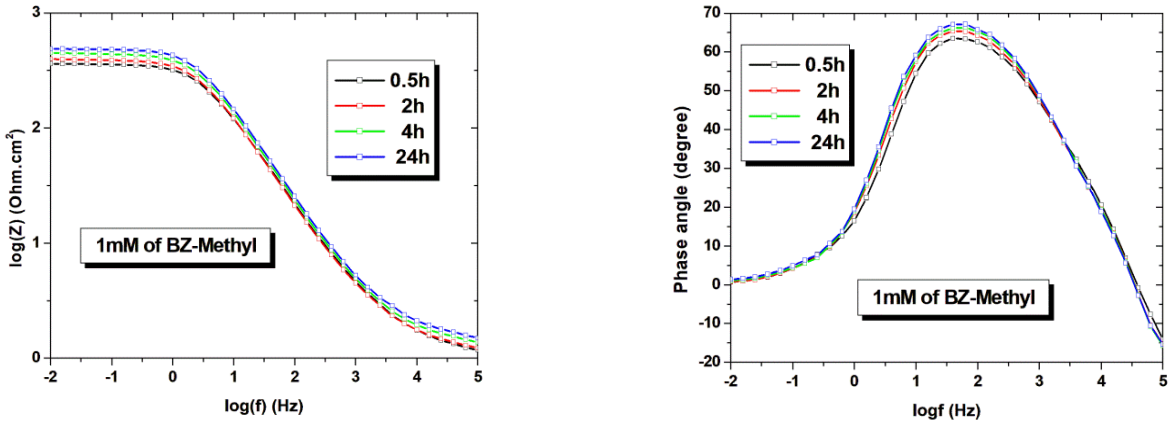

Figure 11. Bode modulus and angle phase plots of E24 steel at different immersion times in 1 M HCl at 293 K.

From Table 3, it's interesting that the values of R_{ct} increase as the immersion time increases, while the CPE_{dl} shows opposite trends. After being submerged for 24 h, R_{ct} is 470.1 Ω·cm^2 and CPE_{dl} is 33.9 μF·cm^{-2}. This suggests that the E24 steel surface attracts BZ-Me molecules to form a protective layer that impedes the charge transfer process [61, 62]. Furthermore, changes in the morphology of the electrode surface due to roughness and other irregularities of E24 steel cause the n value to decrease as the immersion period increases.

Table 3. The values of the descriptor electrochemical impedance parameters E24 steel at different immersion times in 1 M HCl at 293 K.

Time	R_s (Ω·cm^2)	R_{ct} (Ω·cm^2)	CPE_{dl} (μF·cm^{-2})	*n*
0.5	3.961	353.7	45	0.8927
2	2.661	391.9	40.6	0.8645
4	3.566	440.3	36.2	0.8798
24	2.449	470.1	33.9	0.8599

3.4. Adsorption isotherm

Adsorption isotherms are extremely beneficial for comprehending the mechanism beneath organic electrochemical reactions [63]. During this process, molecules attach themselves to iron atoms by interacting with their active sites or previously absorbed intermediate species. Generally, adsorption isotherm models, such as Langmuir, Freundlich, and Temkin, are commonly employed to define the nature of the interactions that occur between metals and inhibitors. Nevertheless, the relationship between the concentrations of C_{inh}/θ and C_{inh} demonstrates a linear correlation, suggesting that the Langmuir adsorption isotherm is followed by BZ-Me's adsorption from 1 M HCl solutions on the E24 steel surface (Figure 12). Table 4 presents the associated adsorption parameters. The correlation coefficient (R^2=0.99) is near 1, proving the reliability of this technique, and it may be calculated using Equation (16) [64]:

$$\frac{C_{inh}}{\theta} = \frac{1}{K_{ads}} + C_{inh} \tag{16}$$

where θ represents the coverage rate, K_{ads} denotes the adsorption constant, and C_{inh} represents the concentration of the inhibitor. The K_{ads} value represents the degree of adsorption capability between the BZ-Me substance and the E24 steel surface. The least squares approach is used to create a straight line for the adsorption parameters computation. The equilibrium constant of the adsorption process is reliant on the standard adsorption-free energy *via* the following Equation (17) [65]:

$$\Delta G^0_{ads} = -RT\ln(55.55K_{ads}) \tag{17}$$

The number 55.55 reflects the concentration of water in the solution, represented in molarity, while R is the universal gas constant (8.314 $J \cdot K^{-1} \cdot mol^{-1}$), and T represents the absolute temperature (298.15 K). Table 5 provides an overview of the relevant adsorption parameters.

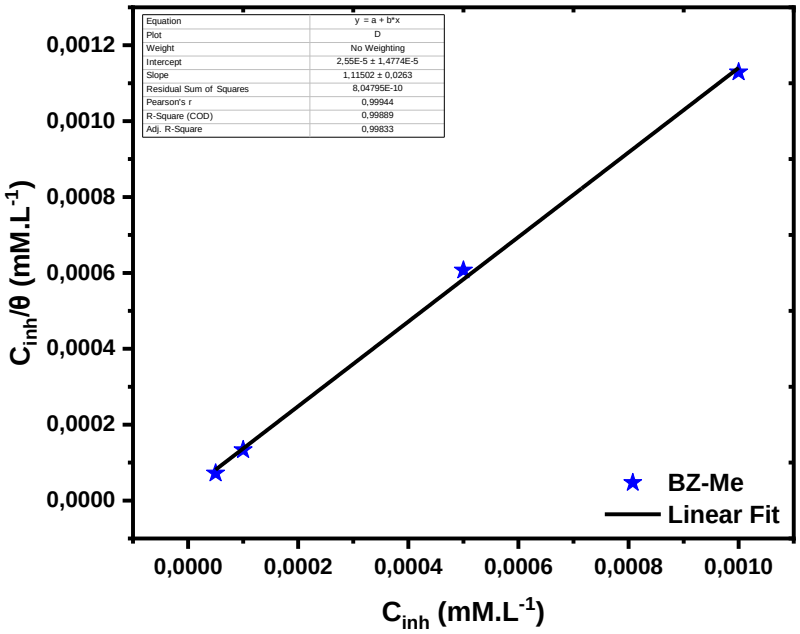

Figure 12. Langmuir isotherm for adsorption of BZ-Me onto the E24 steel in 1 M HCl solution at 293 K.

From this plot, the BZ-Me molecule has a significant inhibitory action and is effectively adsorbed across the E24 steel surface, demonstrated by the higher value of K_{ads} $0.39 \cdot 10^5$ $L \cdot mol^{-1}$. Moreover, the negative adsorption-free energy value reveals the durability and spontaneity of the resulting molecular barrier. A multitude of studies [66–71] show that the adsorption of inhibitors happens *via* physical interactions when the ΔG^0_{ads} values are around –20 $kJ \cdot mol^{-1}$ or less negative. Conversely, if the ΔG^0_{ads} values are near –40 $kJ \cdot mol^{-1}$ or more negative, the adsorption of inhibitors proceeds *via* chemical interactions. Based on the data summarized in Table 4, the adsorption value was between $-20 < \Delta G^0_{ads} < -40$, suggesting that the adsorption process of BZ-Me on E24 steel involves a mix of physical and chemical adsorptions (physio-chemisorption) [72].

Table 4. Adsorption parameters for BZ-Me through the E24 steel in 1 M HCl solution at 293 K.

Inhibitor	**K_{ads} ($L \cdot mol^{-1}$)**	**R^2**	**ΔG^0_{ads}, $kJ \cdot mol^{-1}$**
BZ-Me	$0.39 \cdot 10^5$	0.99	–36.17

3.5. Surface analysis

To understand the act of adsorption of the BZ-Me onto the surface of the E24 steel, we conducted a surface examination using the SEM method. Figure 13 (a, b) reports the scanning electron microscopy (SEM) observations of E24 steel immersed in 1 M HCl alone and with 1 mM of BZ-Me for 24 hours. Upon analyzing the morphology of E24 steel in Figure 13a, we observed clear and distinguishable damage, characterized by visible pits, caused by the aggressive action of hydrochloric acid (HCl). A significant transformation occurred with the addition of 1 mM BZ-Me, as depicted in Figure 13b, where the surface exhibited a much smoother appearance. This improvement can be attributed to the formation of a protective barrier film of BZ-Me species across the surface of the E24 steel [73].

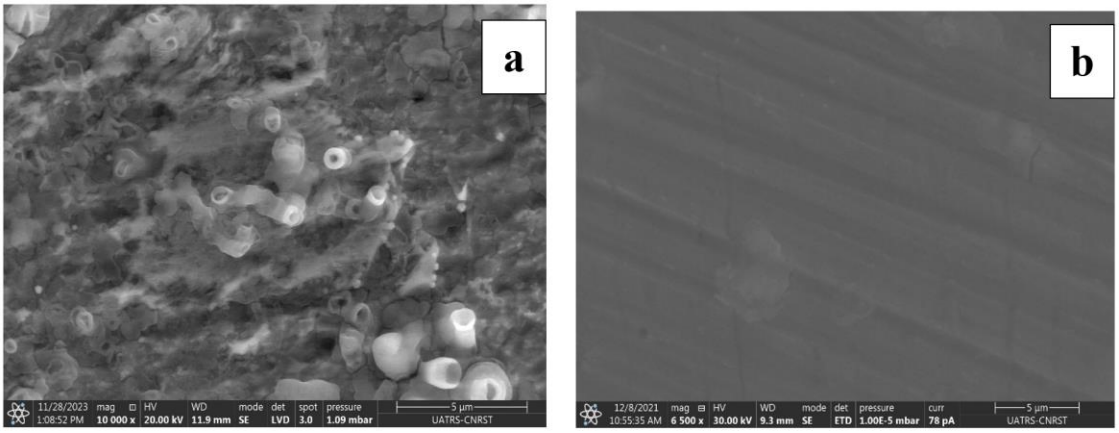

Figure 13. SEM images of E24 steel exposed for 24 hours to 1 M HCl (a) and 1 mM of BZ-Me (b).

In parallel, the energy-dispersive X-ray analysis (EDS) approach determines the composition of a specimen's surface [74]. Figure 14 (a, b) illustrates the energy dispersive X-ray analysis (EDS) spectra of E24 steel immersed in 1 M HCl alone and with the addition of 1 mM BZ-Me. Table 5 provides further details about the weight percentages of the elements.

Based on Figure 14 and the data in Table 5, it is evident that BZ-Me has altered the surface composition of E24 steel, reducing the percentage of certain elements, with some elements no longer detectable due to the BZ-Me film covering them. The carbon percentage notably increased from 1.3% to 2.7%. Additionally, Figure 14b shows a new peak with 0.9% nitrogen, confirming the presence of a surface layer formed by chemical elements from BZ-Me adhering to the metal surface. Moreover, the introduction of corrosion inhibitors led to an increase in iron content from 73.8% to 85.1%, indicating the formation of a protective film. This film acts as a shield, preventing corrosion and reducing iron breakdown or oxidation. The decrease in oxygen (O) levels from 19.9% to 10.4% when inhibitors were present suggests a slowdown in oxide production and oxidation processes. These findings corroborate the conclusions drawn from PDP and EIS tests, supporting the existence of a surface coating that inhibits metal dissolution.

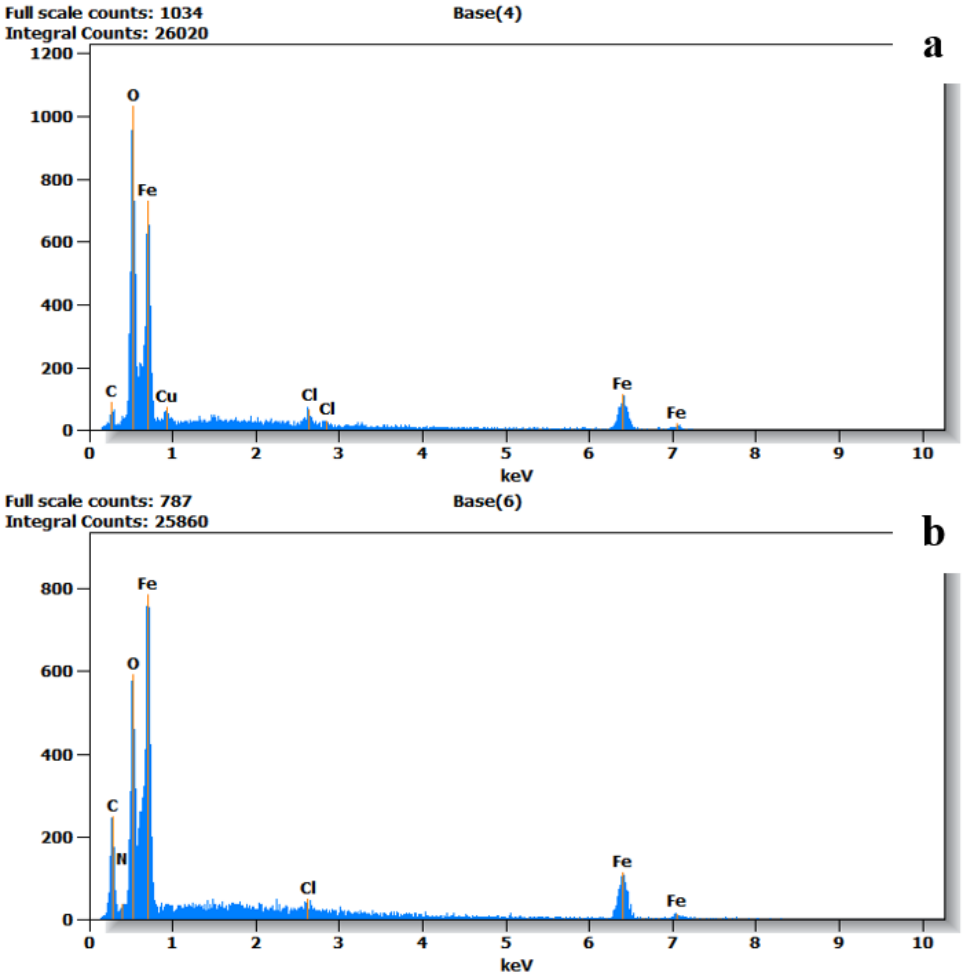

Figure 14. EDX spectra of E24 steel exposed for 24 hours in 1 M HCl (a) and 1 mM of BZ-Me (b).

Table 5. Surface composition (wt%) of E24 steel after immersion of 24 h in 1 M HCl solution without and with 1 mM BZ-Me.

Element (wt%)	1 M HCl	BZ-Me
C	1.3	2.7
N	0.0	0.9
O	19.9	10.4
Cl	1.9	0.9
Fe	73.8	85.1
Cu	3.2	0.0

3.6. DFT Calculations

3.6.1. Frontier molecular orbitals and quantum reactivity descriptors of the BZ-Me

Figure 15 shows the optimized geometry as well as HOMO, LUMO, and molecular electrostatic potentials (MEP) of BZ-Me in its neutral form obtained in the gas phase using DFT at the PBEPBE/6-31G+(d,p). It is observed that the HOMO and LUMO are delocalized over the entire molecule of BZ-Me. The electrostatic potentials at the surface are represented by different colors; red, blue, and green represent the regions of negative, positive, and zero electrostatic potentials respectively. In particular, the negative regions (red color) of MEP are related to electrophilic reactivity, and the positive regions (blue color) are related to nucleophilic reactivity [75]. As seen, the negative electrostatic potentials are localized over the oxygen atoms which are the potential sites for electrophilic attack. However, positive regions are localized around the hydrogen atoms. The green region corresponds to electrostatic potential halfway between the red and the blue and are potential sites for intermolecular interactions.

Table 6 summarizes the values of some quantum chemical parameters for the optimized structure of the BZ-Me inhibitor.

Table 6. The calculated global reactivity descriptors of the BZ-Me in the gas phase at DFT/PBEPBE/6-31+(p,d).

Property	**DFT/PBEPBE/6-31+(p,d)**
	Benzodiazepin
E_{HOMO} (eV)	–5.169
E_{LUMO} (eV)	–2.356
ΔE_{gap} (eV)	2.813
IP (eV)	5.169
EA (eV)	2.356
χ (eV)	3.762
η (eV)	1.406
S (eV^{-1})	0.710
ω^{+} (eV)	3.327
ω^{-} (eV)	7.089
$\Delta E_{back\text{-}donation}$ (eV)	–0.351
ΔN (eV)	0.375
$\Delta\psi$ (eV)	0.198

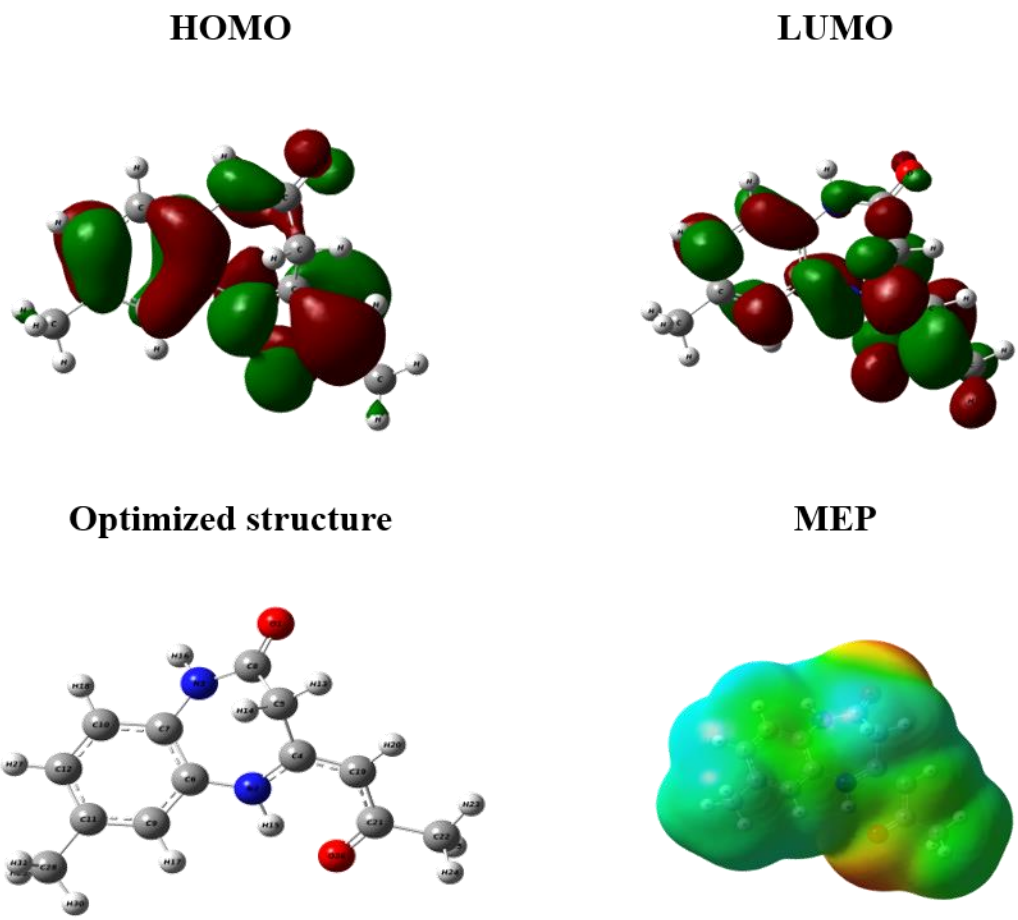

Figure 15. The optimized structures, HOMO, LUMO, and molecular electrostatic potentials (MEP) of BZ-Me in its neutral form obtained in the gas phase using DFT at the PBEPBE/6-31G+(d,p) basis set.

The high E_{HOMO} value for BZ-Me implies its good tendency to donate electrons to the empty d-orbital of the metal while the low E_{LUMO} value indicates that the electrons from the E24 steel surface are easily accepted by BZ-Me molecules. The HOMO–LUMO energy gap (ΔE_{gap}) explains the molecular stability, chemical reactivity, and hardness of the inhibitor [76–78]. In the chemical reactivity theory, the parameters like electronegativity, hardness, and softness have proved to be very useful quantities. The electronegativity of the inhibitor molecules is lower than the iron. Hence, electrons move from BZ-Me molecules with lower electronegativity toward that of a higher value (E24 steel surface) until the equilibrium in chemical potential is reached [77]. To calculate the fraction of electrons transferred, a theoretical value for the electronegativity of bulk iron was used Fe=7 eV, and a global hardness of η=0, by assuming that for a metallic bulk, ionization potential (I)=electron affinity (A), because they are softer than the neutral metallic atoms. Obtained values of ΔN, show that the inhibition efficiency resulting from electron donation agrees with Lukovits's study [79]. If ΔN<3.6, the inhibition efficiency of BZ-Me molecules increases by increasing their electron-donating ability to the metal surface.

Furthermore, the interaction between the inhibitor molecule and the metal surface can be further demonstrated *via* the back donation $\Delta E_{\text{back-donation}}$ energy. The process of back donation is improved if the global hardness is positive and the energy of back donation ($\Delta E_{\text{back-donation}}$) value is negative [80] and this is the case in BZ-Me molecules. Also, the stabilizing energy of a system as it becomes saturated with electrons from the environment is represented by the electrophilicity index (ω) [81]. The ω^- electron-donating power and ω^+ electron-accepting power of the molecules were calculated. It follows that a larger (ω^+) electron-accepting power value corresponds to a better capability of accepting charge, whereas a smaller value of (ω^-) electron-donating power value of a system makes it a better electron donor [80].

3.6.2. Mulliken charge distribution and contour representation of ESP distributions

Figure 16 shows the Mulliken charges and contour representation of ESP distributions of BZ-Me. Mulliken charge distribution offers valuable information regarding the mechanism and mode of inhibition as well adsorption of inhibitor's molecules on the E24 steel surface. It has been stated that as the Mulliken charges of the adsorbed center become more negative, the atom more easily donates its electron to the vacant orbital of the metal [78–82]. It is noted that oxygen atoms (O_1=−0.379; O_{26}=−0.347) have high charge densities and are mainly active centers, which have the strongest ability to bond to the metal surface. This is confirmed by using ESP maps, in which it is possible to visualize the electron distribution, and therefore identify the active centers in the molecule [83]. The contour maps of electron density reveal that oxygen atoms in BZ-Me exhibit favorable interaction sites. Interaction sites surrounded by a dark red contour contribute to forming the bonding interactions between the E24 steel surface and BZ-Me molecules [84]. The dark red color in the contour map of negative potential particularly surrounds oxygen molecules, whereas the light green color is scattered in the positive potential region.

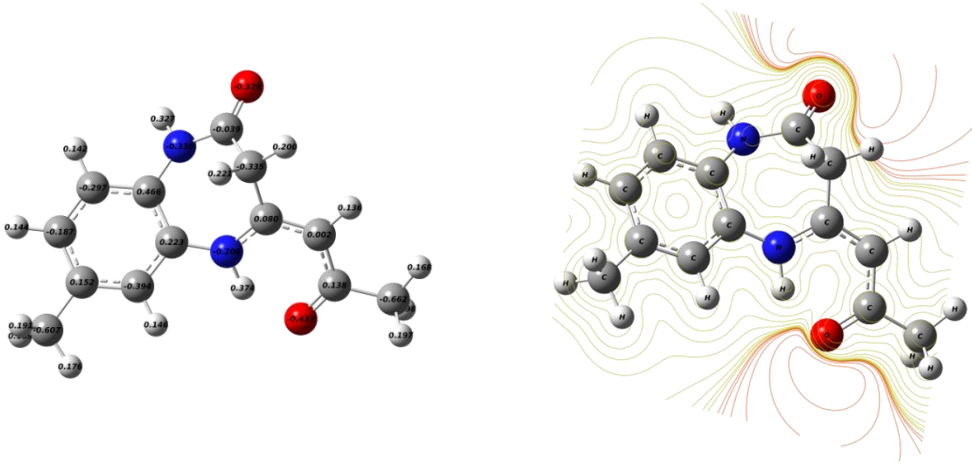

Figure 16. Mulliken charges and ESP distributions for BZ-Me.

3.7. MD modeling results

To further explain the corrosion inhibition mechanism of BZ-Me, the adsorption pattern and the coverage efficiency of the active molecules on the E24 steel surface were investigated *via* MD simulations. The corresponding energy was calculated as follows [85].

$$E_{ads} = E_{inter} = E_{total} - (E_{steel+sol} + E_{inh}) \quad (18)$$

$$E_{binding} = -E_{ads} \quad (19)$$

where E_{ads} is the adsorption energy of the inhibitor molecules on E24 steel surface, E_{total} is the energy of the entire system containing the inhibitor molecules, water molecules, and iron atoms, $E_{steel+sol}$ is the system energy of the iron atoms and water molecules, E_{inh} is the energy of the inhibitor molecules, $E_{binding}$ is the binding energy of the inhibitor molecules on the Fe (110) surface, E_{inter} is the interaction energy between the inhibitor molecules and E24 steel surface. For the adsorption system in this study, E_{ads} and E_{inter} were equal. The side and top views of the final stable configurations of BZ-Me adsorbed on the Fe (110) plane based on MD simulations are shown in Figure 17. The corresponding E_{ads} are listed in Table 7.

In general, molecules adsorbed in a pattern parallel to the metal surface can provide greater coverage and more consistency of the protective film, strengthening the mechanical barrier function and providing a better protection effect [86, 87]. As shown in Figure 17, BZ-Me molecules are almost adsorbed in parallel on the surface of Fe (110). These are due to coordinate bonds formed when inhibitor molecules donate electrons to the unoccupied d-orbital of iron or accept the electrons from iron through molecule heteroatoms.

As shown in Table 7, the E_{ads} of BZ-Me are negative, further suggesting a spontaneous adsorption process. However, a larger $E_{binding}$ suggests that the formed adsorption film is firmer and can improve corrosion protection Generally speaking, a larger $E_{binding}$ indicates a tough binding of the inhibitor molecule to the metal surface, the molecules are inclined to adsorb on the metal surface, exhibiting excellent inhibitive performance [87]. Based on the calculated results, the $E_{binding}$ of BZ-Me molecules is relatively large, manifesting that it has a certain degree of inhibition on E24 steel corrosion in HCl solution.

Table 7. Calculated values of $E_{interaction}$ and $E_{binding}$ (all in kcal/mol) obtained from MD simulations of BZ-Me/Fe (110) surface.

System	$E_{interaction}$	$E_{binding}$
BZ-Me/Fe (110)	–99.2220	99.2220

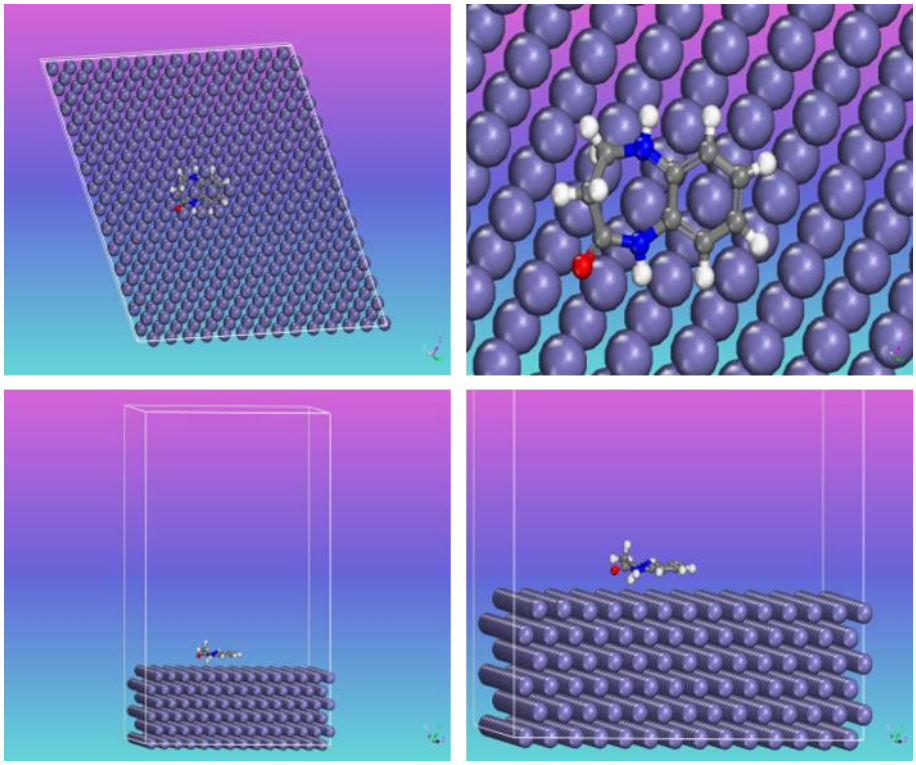

Figure 17. Equilibrium adsorption configuration of BZ-Me over the Fe-surface as determined by MD.

Considering the effect of temperature on MD modeling; all simulation processes were run until the simulation system reached a balance. Temperature fluctuation during simulations is depicted in Figure 18, which demonstrates that the studied systems tend to equilibrium at the end of the simulation process.

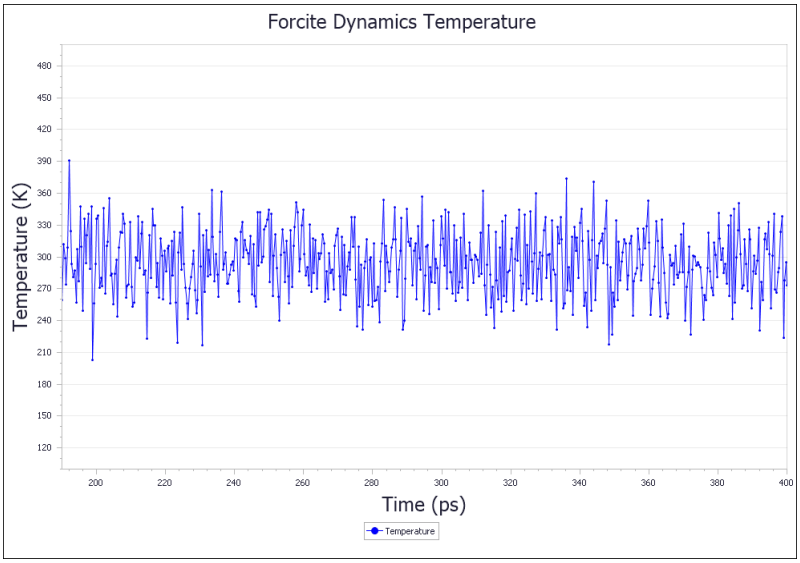

Figure 18. Temperature equilibrium curve for BZ-Me/Fe (110) surface.

Furthermore, to clarify inhibitor–steel interactions, RDF analysis computed from MD trajectory data provides further insights into the mode of action between BZ-Me molecules and Fe (110) surface. In this case, we succeeded in obtaining the calculation of the RDF using [88, 89]:

$$g_{AB}(r) = \frac{1}{\rho B_{local}} \times \frac{1}{N_A} \sum_{i \in A}^{N_A} \sum_{i \in B}^{N_B} \frac{\delta(r_{ij} - r)}{4\pi r^2} \quad (20)$$

where ρB_{local} represents the particle density of B averaged over all shells around the particle.

As was discussed in previous parts, the BZ-Me compound can easily adsorb onto the E24 steel surface. Therefore, efforts were devoted to determining the significant interactions during the adsorption mechanism by measuring the typical bonding length. For this reason, the radial distribution function was calculated for BZ-Me with the help of MD trajectories and depicted in Figure 19. It is well known that the peak occurs at 1–3.5 Å related to small bond length and the kind of interaction is a chemisorption type, while a distance greater than 3.5 Å is associated with physisorption [90]. A look at RDF patterns shows that prominent peaks for Fe–O in BZ-Me molecule are smaller than 3.5 Å (Fe–O; 2.47). This supports the conclusion that a chemical interaction can occur during the adsorption of the BZ-Me onto the steel surface as indicated by the values of ΔG_{ads}=−36.17 kJ/mol.

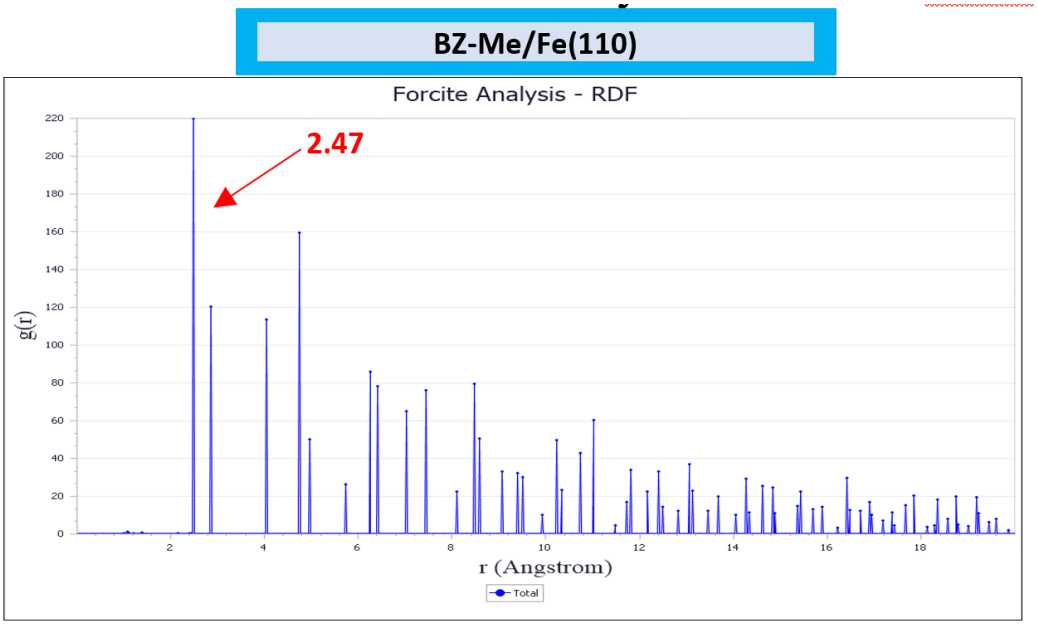

Figure 19. RDF of the BZ-Me on the Fe-surface in a corrosive medium.

4. Conclusion

This study focuses on synthesizing a novel derivative, (*Z*)-7-methyl-4-(2-oxopropylidene)-[1,5]-benzodiazepin-2-one (BZ-Me), belonging to the benzodiazepin-2-one family. BZ-Me acts as a corrosion inhibitor for E24 steel, investigated in aggressive solutions using potentiodynamic polarization (PDP), electrochemical impedance spectroscopy (EIS), and

scanning electron microscopy with energy dispersive spectroscopy (SEM-EDS). Tafel polarization results indicate BZ-Me adheres strongly to E24 steel, exhibiting mixed-type behavior favoring anodic reactions. EIS shows a significant corrosion rate reduction (88.55% at 1 mM BZ-Me) with frequency dispersion described by a constant phase element (CPE_{dl}). Kinetic parameters suggest BZ-Me follows Langmuir adsorption, combining physical and chemical adsorptions on the steel surface. SEM-EDS confirms BZ-Me creates a protective layer on E24 steel, effectively inhibiting corrosion in 1 M HCl, highlighting its potential for diverse industrial applications. Furthermore, the modeling investigations using molecular dynamics (MD) simulations and electronic quantum mechanics (DFT) calculations underscored the interfacial adsorption and formation of a corrosion-resistant layer by the BZ-Me inhibitor on the E24 steel surface, consistent with the experimental findings.

References

1. J.B. Zimmerman, P.T. Anastas, H.C. Erythropel and W. Leitner, Designing for a green chemistry future, *Science*, 2020, **367**, no. 6476, 397–400. doi: 10.1126/science.aay3060
2. A. Belakhdar, H. Ferkous, S. Djellali, R. Sahraoui, H. Lahbib and Y.B. Amor, Corrosion Inhibition Performance of Rosmarinus officinalis Methanolic Extract on Carbon Steel XC48 in Acidic Medium (2 M HCl), *Mater. Biomater. Sci*., 2020, 46–53.
3. R. Idouhli, A. Oukhrib, Y. Koumya, A. Abouelfida, A. Benyaich and A. Benharref, Inhibitory effect of Atlas cedar essential oil on the corrosion of steel in 1 M HCl, *Corros. Rev*., 2018, **36**, 373–384. doi: 10.1515/corrrev-2017-0076
4. A. Molhi, R. Hsissou, M. Damej, A. Berisha, V. Thaçi, A. Belafhaili, M. Benmessaoud, N. Labjar and S. El Hajjaji, Contribution to the corrosion inhibition of C38 steel in 1 M hydrochloric acid medium by a new epoxy resin PGEPPP, *Int. J. Corros. Scale Inhib*., 2021, **10**, no. 1, 399–418. doi: 10.17675/2305-6894-2021-10-1-23
5. A. Molhi, R. Hsissou, M. Damej, A. Berisha, M. Bamaarouf, M. Seydou, M. Benmessaoud and S. El Hajjaji, Performance of two epoxy compounds against corrosion of C38 steel in 1 M HCl: Electrochemical, thermodynamic and theoretical assessment, *Int. J. Corros. Scale Inhib*., 2021, **10**, no. 2, 812–837. doi: 1017675/2305-6894-2021-10-2-21
6. L. Randall, B. Kappel, S. Garattini, E. Mussini and L.O. Randal, *Benzodiazepines*, Raven Press, 1973.
7. J. Landquist, A. Katritzky and C. Rees, *Comprehensive Heterocyclic Chemistry*, Pergamon, Oxford, 1984, **1**, 166–170.
8. R.C. Haris and J.M. Straley, US Patent 1537757, *Chem. Abstr*., 1970, 100054w.
9. I. Racamonde, J.B. Quintana, R. Rodil and R. Cela, Application of polypropylene tubes as single-use and low-cost sorptive extraction materials for the determination of benzodiazepines and zolpidem in water samples, *Microchem. J*., 2015, **119**, 58–65. doi: 10.1016/j.microc.2014.10.011

10. C. Salzman, Benzodiazepine treatment of panic and agoraphobic symptoms: Use, dependence, toxicity, abuse, *J. Psychiatr. Res*., 1993, **27**, 97–110. doi: 10.1016/0022-3956(93)90021-s
11. K. Chkirate, J. Akachar, B. Hni, T. Hökelek, E.H. Anouar, A. Talbaoui, J.T. Mague, N.K. Sebbar, A. Ibrahimi and E.M. Essassi, Synthesis, spectroscopic characterization, crystal structure, DFT, ESI-MS studies, molecular docking and *in vitro* antibacterial activity of 1,5-benzodiazepin-2-one derivatives, *J. Mol. Struct*., 2022, **1247**, 131188. 10.1016/j.molstruc.2021.131188
12. M. Reda, L. El Ghayati and E.M. Essassi, Les 1,5-benzodiazepines: syntheses et reactivites, *J. Mar. Chim. Heterocycl*., 2018, **17**, no. 1, 41. doi: 10.48369/IMIST.PRSM/jmch-v17i1.11341
13. B. El Ibrahimi, Atomic-scale investigation onto the inhibition process of three 1,5-benzodiazepin-2-one derivatives against iron corrosion in acidic environment, *Colloid Interface Sci. Commun*., 2020, **37**, 100279. doi: 10.1016/j.colcom.2020.100279
14. J. Sebhaoui, Y. El Bakri, Y. El Aoufir, E.H. Anouar, A. Guenbour, A.A. Nasser and E.M. Essassi, Synthesis, NMR characterization, DFT and anti-corrosion on carbon steel in 1 M HCl of two novel 1,5-benzodiazepines, *J. Mol. Struct*., 2019, **1182**, 123–130. doi: 10.1016/j.molstruc.2019.01.037
15. T. Laabaissi, M. Rbaa, F. Benhiba, Z. Rouifi, U.P. Kumar, F. Bentiss, H. Oudda, B. Lakhrissi, I. Warad and A. Zarrouk, Insight into the corrosion inhibition of new benzodiazepine derivatives as highly efficient inhibitors for mild steel in 1 M HCl: Experimental and theoretical study, *Colloids Surf., A*, 2021, **629**, 127428. doi: 10.1016/j.colsurfa.2021.127428
16. W. Kohn and L.J. Sham, Self-Consistent Equations Including Exchange and Correlation Effects, *Phys. Rev*., 1965, **140**, A1133–A1138. doi: 10.1103/PhysRev.140.A1133
17. P. Hohenberg and W. Kohn, Inhomogeneous Electron Gas, *Phys. Rev*., 1964, **136**, B864–B871. doi: 10.1103/PhysRev.136.B864
18. C. Lee, W. Yang and R.G. Parr, Development of the Colle-Salvetti correlation-energy formula into a functional of the electron density, *Phys. Rev. B*, 1988, **37**, 785–789. doi: 10.1103/PhysRevB.37.785
19. J.-D. Chai and M. Head-Gordon, Long-range corrected hybrid density functionals with damped atom–atom dispersion corrections, *Phys. Chem. Chem. Phys*., 2008, **10**, no. 44, 6615. doi: 10.1039/B810189B
20. M.J. Frisch, G.W. Trucks, H.B. Schlegel, G.E. Scuseria, M.A. Robb, J.R. Cheeseman, G. Scalmani, V. Barone, G.A. Petersson, H. Nakatsuji, X. Li, M. Caricato, A. Marenich, J. Bloino, B.G. Janesko, R. Gomperts, B. Mennucci, H.P. Hratchian, J.V. Ortiz, A.F. Izmaylov, J.L. Sonnenberg, D. Williams-Young, F. Ding, F. Lipparini, F. Egidi, J. Goings, B. Peng, A. Petrone, T. Henderson, D. Ranasinghe, V.G. Zakrzewski, J. Gao, N. Rega, G. Zheng, W. Liang, M. Hada, M. Ehara, K. Toyota, R. Fukuda, J. Hasegawa, M. Ishida, T. Nakajima, Y. Honda, O. Kitao, H. Nakai, T. Vreven, K. Throssell, J.A. Montgomery, Jr., J.E. Peralta, F. Ogliaro, M. Bearpark, J.J. Heyd, E. Brothers,

K.N. Kudin, V.N. Staroverov, T. Keith, R. Kobayashi, J. Normand, K. Raghavachari, A. Rendell, J.C. Burant, S.S. Iyengar, J. Tomasi, M. Cossi, J.M. Millam, M. Klene, C. Adamo, R. Cammi, J.W. Ochterski, R.L. Martin, K. Morokuma, O. Farkas, J.B. Foresman and D.J. Fox, *Gaussian 09, Revision A.02*, Gaussian, Inc., Wallingford CT, 2016.

21. A. Chraka, N.B. Seddik, I. Raissouni, J. Kassout, M. Choukairi, M. Ezzaki, O. Zaraali, H. Belcadi, F. Janoub, A. Ibn Mansour, M. Benmessaoud and D. Bouchta, Electrochemical explorations, SEM/EDX analysis, and quantum mechanics/molecular simulations studies of sustainable corrosion inhibitors on the Cu-Zn alloy in 3% NaCl solution, *J. Mol. Liq*., 2023, **387**, 122715. doi: 10.1016/j.molliq.2023.122715
22. N. Metropolis and S. Ulam, The Monte Carlo Method, *J. Am. Stat. Assoc*., 1949, **44**, no. 247, 335–341.
23. N. Metropolis, A.W. Rosenbluth, M.N. Rosenbluth, A.H. Teller and E. Teller, Equation of State Calculations by Fast Computing Machines, *J. Chem. Phys*., 1953, **21**, 1087–1092. doi: 10.1063/1.1699114
24. M. Belhadi, M. Oubahou, I. Hammoudan, A. Chraka, M. Chafi and S. Tighadouini, A comprehensive assessment of carbon steel corrosion inhibition by 1,10-phenanthroline in the acidic environment: insights from experimental and computational studies, *Environ. Sci. Pollut. Res*., 2023. doi: 10.1007/s11356-023-27582-1
25. M. Abouchane, R. Hsissou, A. Chraka, A. Molhi, M. Damej, K. Tassaoui, A. Berisha, M. Seydou, B.O. Elemine and M. Benmessaoud, Synthesis and Characterization of New Macromolecular Epoxy Resin as an Effective Corrosion Inhibitor for C38 Steel in 1 M HCl Medium: Electrochemical Insights, Surface Morphological and Computational Approaches, *J. Bio Tribo Corros*., 2024, **10**, 21. doi: 10.1007/s40735-024-00824-6
26. H. Belcadi, A. Chraka, S. El Amrani, I. Raissouni, A. Moukhles, S. Zantar, L. Toukour and A.I. Mansour, Investigation and Valorization of the Moroccan *Salvia Officinalis* L. Essential Oil: Phytochemistry, Potential in Corrosion Inhibition, Antibacterial Activity, and Theoretical Modeling, *J. Bio Tribo Corros*., 2023, **9**, 50. doi: 10.1007/s40735-023-00769-2
27. H. Sun, P. Ren and J.R. Fried, The COMPASS force field: parameterization and validation for phosphazenes, *Comput. Theor. Polym. Sci*., 1998, **8**, 229–246. doi: 10.1016/S1089-3156(98)00042-7
28. A. Chraka, I. Rais souni, N.B. Seddik, S. Khayar, A.I. Mansour, S. Tazi, F. Chaouket and D. Bouchta, Identification of Potential Green Inhibitors Extracted from *Thymbra capitata* (L.) Cav. for the Corrosion of Brass in 3% NaCl Solution: Experimental, SEM–EDX Analysis, DFT Computation and Monte Carlo Simulation Studies, *J. Bio Tribo Corros*., 2020, **6**, 80. doi: 10.1007/s40735-020-00377-4
29. A. Chraka, I. Raissouni, N.B. Seddik, S. Khayar, S. El Amrani, M. El Hadri, F. Chaouket and D. Bouchta, *Croweacin* and *Ammi visnaga* (L.) Lam Essential Oil derivatives as green corrosion inhibitors for brass in 3% NaCl medium: Quantum

Mechanics investigation and Molecular Dynamics Simulation Approaches, *Mediterr. J. Chem.*, 2020, **10**, 378. doi: 10.13171/mjc10402004281338ac
30. A.A. Al-Amiery, N. Betti, W.N.R.W. Isahak, W.K. Al-Azzawi and W.M.N.W. Nik, Exploring the Effectiveness of Isatin–Schiff Base as an Environmentally Friendly Corrosion Inhibitor for Mild Steel in Hydrochloric Acid, *Lubricants*, 2023, **11**, no. 5, 211. doi: 10.3390/lubricants11050211
31. H.H. Hassan, E. Abdelghani and M.A. Amin, Inhibition of mild steel corrosion in hydrochloric acid solution by triazole derivatives. Part I. Polarization and EIS studies, *Electrochim. Acta*., 2007, **52**, 6359–6366. doi: 10.1016/j.electacta.2007.04.046
32. M.A. Amin, S.S. Abd El-Rehim, E.E.F. El-Sherbini and R.S. Bayoumi, The inhibition of low carbon steel corrosion in hydrochloric acid solutions by succinic acid. Part I. Weight loss, polarization, EIS, PZC, EDX and SEM studies, *Electrochim. Acta*., 2007, **52**, no. 11, 3588–3600. doi: 10.1016/j.electacta.2006.10.019
33. M. Lebrini, F. Robert, H. Vezin and C. Roos, Electrochemical and quantum chemical studies of some indole derivatives as corrosion inhibitors for C38 steel in molar hydrochloric acid, *Corros. Sci*., 2010, **52**, no. 10, 3367–3376. doi: 10.1016/j.corsci.2010.06.009
34. G.D. Pai, M.R. Rathod, S.K. Rajappa and A.A. Kittur, Effect of *tabebuia heterophylla* plant leaves extract on corrosion protection of low carbon steel in 1 M HCl medium: Electrochemical, quantum chemical and surface characterization studies., *Res. Surf. Inter*., 2024, **15**, 100203. doi: 10.1016/j.rsurfi.2024.100203
35. J. Aljourani, K. Raeissi and M.A. Golozar, Benzimidazole and its derivatives as corrosion inhibitors for mild steel in 1 M HCl solution, *Corros. Sci*., 2009, **51**, no. 8, 1836–1843. doi: 10.1016/j.corsci.2009.05.011
36. K. Chkirate, K. Azgaou, H. Elmsellem, B. El Ibrahimi, N.K. Sebbar, E.H. Anouar, M. Benmessaoud, S. El Hajjaji and E.M. Essassi, Corrosion Inhibition Potential of 2-[(5-methylpyrazol-3-yl)methyl]benzimidazole against carbon steel corrosion in 1 M HCl solution: Combining Experimental and Theoretical Studies, *J. Mol. Liq*., 2021, **321**, 114750. doi: 10.1016/j.molliq.2020.114750
37. K. Tassaoui, A. Al-Shami, M. Damej, A. Molhi, O. Mounkachi and M. Benmessaoud, Contribution to the corrosion inhibitors of copper-nickel (Cu-30Ni) in 3% NaCl solution by two new molecules of triazole: Electrochemical and theoretical studies, *J. Mol. Struct*., 2023, **1291**, 135836. doi: 10.1016/j.molstruc.2023.135836
38. G.A. Zhang, X.M. Hou, B.S. Hou and H.F. Liu, Benzimidazole derivatives as novel inhibitors for the corrosion of mild steel in acidic solution: Experimental and theoretical studies, *J. Mol. Liq*., 2019, **278**, 413–427. doi: 10.1016/j.molliq.2019.01.060
39. M. Chevalier, M. Lebrini, F. Robert, S. Sutour, F. Tomi, C. Jama, F. Bentiss and C. Roos, Investigation of Corrosion Inhibition Efficiency of Amazonian Tree Alkaloids Extract for C38 steel in 1 M Hydrochloric Media, *Int. J. Electrochem. Sci*., 2019, **14**, no. 2, 1208–1223. doi: 10.20964/2019.02.38

40. M. Lebrini, M. Lagrenée, H. Vezin, M. Traisnel and F. Bentiss, Experimental and theoretical study for corrosion inhibition of mild steel in normal hydrochloric acid solution by some new macrocyclic polyether compounds, *Corros. Sci*., 2007, **49**, 2254–2269. doi: 10.1016/j.corsci.2006.10.029
41. H.M.A. El-Lateef, M.A. Abo-Riya and A.H. Tantawy, Empirical and quantum chemical studies on the corrosion inhibition performance of some novel synthesized cationic gemini surfactants on carbon steel pipelines in acid pickling processes, *Corros. Sci*., 2016, **108**, 94–110. doi: 10.1016/j.corsci.2016.03.004
42. M. Damej, A. Molhi, K. Tassaoui, B. El Ibrahimi, Z. Akounach, A.A. Addi, S. El hajjaji and M. Benmessaoud, Experimental and Theoretical Study to Understand the Adsorption Process of p-Anisidine and 4-Nitroaniline for the Dissolution of C38 Carbon Steel in 1 M HCl, *ChemistrySelect*, 2022, **7**, e202103192. doi: 10.1002/slct.202103192
43. F. Wang and Z. Guo, Facile synthesis of superhydrophobic three-metal-component layered double hydroxide films on aluminum foils for highly improved corrosion inhibition, *New J. Chem*., 2019, **43**, no. 5, 2289–2298. doi: 10.1039/C8NJ05732J
44. W. Al Garadi, K. Jrajri, M. El Faydy, F. Benhiba, L. El Ghayati, N.K. Sebbar, E.M. Essassi, I. Warad, A. Guenbour, A. Bellaouchou, C. Jama and A. Alsalme, A. Zarrouk, 4-phenyl-decahydro-1*H*-1,5-benzodiazepin-2-one as novel and effective corrosion inhibitor for carbon steel in 1 M HCl solution: A combined experimental and empirical studies, *J. Indian Chem. Soc*., 2022, **99**, no. 11, 100742. doi: 10.1016/j.jics.2022.100742
45. M. Faustin, A. Maciuk, P. Salvin, C. Roos and M. Lebrini, Corrosion inhibition of C38 steel by alkaloids extract of *Geissospermum laeve* in 1 M hydrochloric acid: Electrochemical and phytochemical studies, *Corros. Sci*., 2015, **92**, 287–300. doi: 10.1016/j.corsci.2014.12.005
46. A. Macías, Comparison of different electrochemical techniques for corrosion-rate determination of zinc-coated reinforcements in simulated concrete pore solutions, *Mater. Struct*., 1991, **24**, 456–465. doi: 10.1007/BF02472018
47. H. Fakhry, M. El Faydy, F. Benhiba, M. Bouassiria, T. Laabaissi, M. Allali, R. Touir, H. Oudda, C. Jama, I. Warad, A. Alsalme and A. Zarrouk, Experimental, DFT studies and molecular dynamic simulation on the corrosion inhibition of carbon steel in 1 M HCl by two newly synthesized 8-hydroxyquinoline derivatives, *J. Indian Chem. Soc*., 2022, **99**, no. 12, 100701. doi: 10.1016/j.jics.2022.100701
48. A. El-Yaktini, A. Lachiri, M. El-Faydy, F. Benhiba, H. Zarrok, M. El-Azzouzi, M. Zertoubi, M. Azzi, B. Lakhrissi and A. Zarrouk, Practical and Theoretical Study on the Inhibitory Influences of New Azomethine Derivatives Containing an 8-Hydroxyquinoline Moiety for the Corrosion of Carbon Steel in 1 M HCl, *Orient. J. Chem*., 2018, **34**, 3016–3029. doi: 10.13005/ojc/340643
49. D.A. López, S.N. Simison and S.R. de Sánchez, The influence of steel microstructure on CO_2 corrosion. EIS studies on the inhibition efficiency of benzimidazole, *Electrochim. Acta*, 2003, **48**, no. 7, 845–854. doi: 10.1016/S0013-4686(02)00776-4

50. F. Bouhlal, N. Labjar, F. Abdoun, A. Mazkour, M. Serghini-Idrissi, M. El Mahi, E.M. Lotfi, A. Skalli and S. El Hajjaji, Chemical and electrochemical studies of the inhibition performance of hydro-alcoholic extract of used coffee grounds (HECG) for the corrosion of C38 steel in 1 M hydrochloric acid, *Egypt. J. Pet*., 2020, **29**, no. 1, 45–52. doi: 10.1016/j.ejpe.2019.10.003
51. M. Yadav, S. Kumar, R.R. Sinha, I. Bahadur and E.E. Ebenso, New pyrimidine derivatives as efficient organic inhibitors on mild steel corrosion in acidic medium: Electrochemical, SEM, EDX, AFM and DFT studies, *J. Mol. Liq*., 2015, **211**, 135–145. doi: 10.1016/j.molliq.2015.06.063
52. M. Yadav, L. Gope, N. Kumari and P. Yadav, Corrosion inhibition performance of pyranopyrazole derivatives for mild steel in HCl solution: Gravimetric, electrochemical and DFT studies, *J. Mol. Liq*., 2016, **216**, 78–86. doi: 10.1016/j.molliq.2015.12.106
53. K. Tassaoui, M. Damej, A. Molhi, A. Berisha, M. Errili, S. Ksama, V. Mehmeti, S. El Hajjaji and M. Benmessaoud, Contribution to the corrosion inhibition of Cu–30Ni copper–nickel alloy by 3-amino-1,2,4-triazole-5-thiol (ATT) in 3% NaCl solution. Experimental and theoretical study (DFT, MC and MD), *Int. J. Corros. Scale Inhib*., 2022, **11**, no. 1, 221–244. doi: 10.17675/2305-6894-2022-11-1-12
54. T. Yan, S. Zhang, L. Feng, Y. Qiang, L. Lu, D. Fu, Y. Wen, J. Chen, W. Li and B. Tan, Investigation of imidazole derivatives as corrosion inhibitors of copper in sulfuric acid: Combination of experimental and theoretical researches, *J. Taiwan Inst Chem. Eng*., 2020, **106**, 118–129. doi: 10.1016/j.jtice.2019.10.014
55. C. Cao, On electrochemical techniques for interface inhibitor research, *Corros. Sci*., 1996, **38**, no. 12, 2073–2082. doi: 10.1016/S0010-938X(96)00034-0
56. H. Bouammali, E.H. Loukili, H. Elmsellem, S. Jerdioui, K. Bekkouch, A. Aouniti, R. Salghi, C. Jama, F. Bentiss and B. Hammouti., Potential anticorrosive effect of hexamethylenediamine Penta(methylphosphonic) acid on c-steel in hydrochloric acid Solution: An experimental study with DFTB and molecular dynamics simulations, *Mor. J. Chem*., 2024, **12**, no. 2, 830–853. doi: 10.48317/IMIST.PRSM/morjchem-v12i2.47169
57. M. Damej, D. Chebabe, M. Benmessaoud, A. Dermaj, H. Erramli, N. Hajjaji and A. Srhiri, Corrosion inhibition of brass in 3% NaCl solution by 3-methyl-1,2,4-triazol-5-thione, *Corros. Eng., Sci. Technol*., 2015, **50**, no. 2, 103–107. doi: 10.1179/1743278214Y.0000000207
58. B.O. Abdelwedoud, M. Damej, K. Tassaoui, A. Berisha, H. Tachallait, K. Bougrin, V. Mehmeti and M. Benmessaoud, Inhibition effect of *N*-propargyl saccharin as corrosion inhibitor of C38 steel in 1 M HCl, experimental and theoretical study, *J. Mol. Liq*., 2022, **354**, 118784. doi: 10.1016/j.molliq.2022.118784
59. K. Azgaou, M. Damej, S. El Hajjaji, N.K. Sebbar, H. Elmsellem, B. El Ibrahimi and M. Benmessaoud, Synthesis and characterization of *N*-(2-aminophenyl)-2-(5-methyl-1*H*-pyrazol-3-yl) acetamide (AMPA) and its use as a corrosion inhibitor for C38 steel in

1 M HCl. Experimental and theoretical study, *J. Mol. Struct*., 2022, **1266**, 133451. doi: 10.1016/j.molstruc.2022.133451

60. M. Damej, M. Benmessaoud, S. Zehra, S. Kaya, H. Lgaz, A. Molhi, N. Labjar, S. El Hajjaji, A.A. Alrashdi and H.-S. Lee, Experimental and theoretical explorations of S-alkylated mercaptobenzimidazole derivatives for use as corrosion inhibitors for carbon steel in HCl, *J. Mol. Liq*., 2021, **331**, 115708. doi: 10.1016/j.molliq.2021.115708
61. M. Chafiq, A. Chaouiki, M. Damej, H. Lgaz, R. Salghi, I.H. Ali, M. Benmessaoud, S. Masroor and I.-M. Chung, Bolaamphiphile-class surfactants as corrosion inhibitor model compounds against acid corrosion of mild steel, *J. Mol. Liq*., 2020, **309**, 113070. doi: 10.1016/j.molliq.2020.113070
62. M. Damej, R. Hsissou, A. Berisha, K. Azgaou, M. Sadiku, M. Benmessaoud, N. Labjar and S. El hajjaji, New epoxy resin as a corrosion inhibitor for the protection of carbon steel C38 in 1 M HCl. experimental and theoretical studies (DFT, MC, and MD), *J. Mol. Struct*., 2022, **1254**, 132425. doi: 10.1016/j.molstruc.2022.132425
63. H.B. Ouici, O. Benali, Y. Harek, S.S. Al-Deyab, L. Larabi and B. Hammouti, Influence of the 2-Mercapto-1-Methyl Imidazole (MMI) on the Corrosion Inhibition of Mild Steel in 5% HCl, *Int. J. Electrochem Sci*., 2012, **7**, no. 3, 2304–2319. doi: 10.1016/S1452-3981(23)13881-8
64. M. Errili, A. Al Maofari, K. Tassaoui, M. Damej, Z. Lakbaibi, A. Et-Tahir, S. El Hajjaji and M. Benmessaoud, Electrochemical and theoretical (DFT, MC, MD) evaluation of a new compound based on mercaptobenzimidazole against corrosion of Cu–30Ni in a 3% NaCl solution, *Int. J. Corros. Scale Inhib*., 2023, **12**, 458–476. doi: 10.17675/2305-6894-2023-12-2-5
65. M. Abouchane, R. Hsissou, A. Molhi, M. Damej, K. Tassaoui, A. Berisha, A. Chraka and M. Benmessaoud, Exploratory Experiments Supported by Modeling Approaches for TGEEA New Epoxy Resin as a Contemporary Anti-corrosion Material for C38 Steel in 1.0 M HCl, *J. Fail. Anal. and Preven*., 2023, **23**, 1765–1781. doi: 10.1007/s11668-023-01705-9
66. W. Zeng, Y. Xu, P. Ge, W. Xiao, Q. Liu, Z. Gao and Y. Yan, *Ipomoea batatas* leaves extract as a green corrosion inhibitor for Q235 steel in HCl solution, *Int. J. Electrochem. Sci*., 2021, **16**, no. 10, 211031. doi: 10.20964/2021.10.40
67. R.T. Loto, Surface coverage and corrosion inhibition effect of *Rosmarinus officinalis* and zinc oxide on the electrochemical performance of low carbon steel in dilute acid solutions, *Results Phys*., 2018, **8**, 172–179. doi: 10.1016/j.rinp.2017.12.003
68. M. Damej, S. Kaya, B. El Ibrahimi, H.-S. Lee, A. Molhi, G. Serdaroğlu, M. Benmessaoud, I.H. Ali, S. El Hajjaji and H. Lgaz, The corrosion inhibition and adsorption behavior of mercaptobenzimidazole and bis-mercaptobenzimidazole on carbon steel in 1.0 M HCl: Experimental and computational insights, *Surf. Interfaces*, 2021, **24**, 101095. doi: 10.1016/j.surfin.2021.101095
69. J. Haque, V. Srivastava, D.S. Chauhan, H. Lgaz and M.A. Quraishi, Microwave-Induced Synthesis of Chitosan Schiff Bases and Their Application as Novel and Green

Corrosion Inhibitors: Experimental and Theoretical Approach, *ACS Omega*, 2018, **3**, no. 5, 5654–5668. doi: 10.1021/acsomega.8b00455

70. A. Singh, K. Ansari, M. Quraishi and H. Lgaz, Effect of Electron Donating Functional Groups on Corrosion Inhibition of J55 Steel in a Sweet Corrosive Environment: Experimental, Density Functional Theory, and Molecular Dynamic Simulation, *Materials*, 2018, **12**, no. 1, 17. doi: 10.3390/ma12010017
71. B.O. Abdelwedoud, K. Tassaoui, A. Chraka, M. Damej, A. Berisha, H. Tachallait, K. Bougrin, V. Mehmeti and M. Benmessaoud, Novel saccharin derivatives are inhibitors for carbon steel corrosion in 1 M HCl: electrochemical, thermodynamic and theoretical assessment, *Int. J. Corros. Scale Inhib*., 2023, **12**, no. 4, 1819–1848. doi 10.17675/2305-6894-2023-12-4-22
72. M. Damej, M. Benmessaoud, S. Zehra, S. Kaya, H. Lgaz, A. Molhi, N. Labjar, S. El Hajjaji, A.A. Alrashdi and H.-S. Lee, Experimental and theoretical explorations of S-alkylated mercaptobenzimidazole derivatives for use as corrosion inhibitors for carbon steel in HCl, *J. Mol. Liq*., 2021, **331**, 115708. doi: 10.1016/j.molliq.2021.115708 [Same as Ref. 60]
73. N. El-Aouni, O. Dagdag, A. El Amri, H. Kim, R. Haldhar, S.-C. Kim, N. Dkhireche, A. El Bachiri, A. Berisha and M. Rafik, Synthesis, structural characterization and anticorrosion properties of a new hexafunctional epoxy prepolymer based on urea and phosphorus trichloride for E24 carbon steel in 1.0 M HCl, *Colloids Surf*., *A*, 2024, **682**, 132963. doi: 10.1016/j.colsurfa.2023.132963
74. R. Hsissou, O. Dagdag, S. Abbout, F. Benhiba, M. Berradi, M. El Bouchti, A. Berisha, N. Hajjaji and A. Elharfi, Novel derivative epoxy resin TGETET as a corrosion inhibition of E24 carbon steel in 1.0 M HCl solution. Experimental and computational (DFT and MD simulations) methods, *J. Mol. Liq*., 2019, **284**, 182–192. doi: 10.1016/j.molliq.2019.03.180
75. Y. Umar and S. Abdalla, Experimental FTIR and Theoretical Investigation of the Molecular Structure and Vibrational Spectra of Terephthaloyl Chloride by Density Functional Theory, *IOSR J. Appl. Chem*., 2015, **8**, 26–34. doi: 10.9790/5736-08912634
76. O.F. Akinyele, A.S. Adekunle, A.A. Akinmuyisitan, S.S. Durodola, O.E. Oyeneyin, N.D. Ojo and L.O. Olasunkanmi, Adsorption, synergistic inhibitive potentials and quantum chemical studies of (E)-1-(2-((2,4-dimethoxyphenyl)diazenyl)phenyl)-2-hydroxy-2-phenylethan-1-one as mild steel anticorrosion agent in acidic medium, *Results Surf. Interfaces*, 2023, **12**, 100128. doi: 10.1016/j.rsurfi.2023.100128
77. H.T. Rahal, A.M. Abdel-Gaber and G.O. Younes, Inhibition of Steel Corrosion in Nitric Acid by Sulfur Containing Compounds, *Chem. Eng. Commun*., 2016, **203**, no. 4, 435–445. doi: 10.1080/00986445.2015.1017636
78. M.Y. El Sayed, A.M. Abdel-Gaber and H.T. Rahal, Safranin – A Potential Corrosion Inhibitor for Mild Steel in Acidic Media: A Combined Experimental and Theoretical Approach, *J. Fail. Anal. and Prevent*., 2019, **19**, 1174–1180. doi: 10.1007/s11668-019-00719-6

79. I. Lukovits, E. Kálmán and F. Zucchi, Corrosion Inhibitors – Correlation between Electronic Structure and Efficiency, *Corrosion*, 2001, **57**, no. 1, 3–8. doi: 10.5006/1.3290328
80. F. Iorhuna, A.M. Ayuba, A.T. Nyijime, M. Hussain and M. Ibrahim, Comparative Study of Halogen Substituted Isocyanatophosphine as an Adsorptive Inhibitor on Al (110) Crystal Surface, using Density Functional Theory, *Prog. Chem. Biochem. Res*., 2023, **6**, 211–228. doi: 10.48309/pcbr.2023.407104.1266
81. F. Iorhuna, M.A. Ayuba and A.S. Muhammad, Computational Studies on the Corrosion Inhibition of Mild Steel Using Pyrimidine Derivatives, *Adv. J. Chem., Sect. B*, 2023, **5**, 244–260. doi: 10.48309/ajcb.2023.398019.1173
82. S. Xia, M. Qiu, L. Yu, F. Liu and H. Zhao, Molecular dynamics and density functional theory study on relationship between structure of imidazoline derivatives and inhibition performance, *Corros. Sci*., 2008, **50**, no. 7, 2021–2029. doi: 10.1016/j.corsci.2008.04.021
83. H. Bourzi, R. Oukhrib, B. El Ibrahimi, H.A. Oualid, Y. Abdellaoui, B. Balkard, S. El Issami, M. Hilali, L. Bazzi and C. Len, Furfural Analogs as Sustainable Corrosion Inhibitors – Predictive Efficiency Using DFT and *Monte Carlo* Simulations on the Cu(111), Fe(110), Al(111) and Sn(111) Surfaces in Acid Media, *Sustainability*, 2020, **12**, no. 8, 3304. doi: 10.3390/su12083304
84. A. Iruthayaraj, K. Chinnasamy, K.K. Jha, P. Munshi, M.S. Pavan and P. Kumaradhas, Topology of electron density and electrostatic potential of HIV reverse transcriptase inhibitor zidovudine from high resolution X-ray diffraction and charge density analysis, *J. Mol. Struct*., 2019, **1180**, 683–697. doi: 10.1016/j.molstruc.2018.11.098
85. O.F. Akinyele, A.S. Adekunle, A.A. Akinmuyisitan, S.S. Durodola, O.E. Oyeneyin, N.D. Ojo and L.O. Olasunkanmi, Adsorption, synergistic inhibitive potentials and quantum chemical studies of (E)-1-(2-((2,4-dimethoxyphenyl)diazenyl)phenyl)-2-hydroxy-2-phenylethan-1-one as mild steel anticorrosion agent in acidic medium, *Results Surf. Interfaces*, 2023, **12**, 100128. doi: 10.1016/j.rsurfi.2023.100128
86. B. Lin, X. Zhou, T. Duan, C. Zhao, J. Zhu and Y. Xu, Experimental and theoretical study on corrosion inhibition and adsorption performance of *Ipomoea batatas* L. leaf extract for mild steel, *Arabian J. Chem*., 2024, **17**, no. 1, 105410. doi: 10.1016/j.arabjc.2023.105410
87. X. Zhang, L. Yang, Y. Zhang, B. Tan, X. Zheng and W. Li, Combined electrochemical/surface and theoretical assessments of Rosa laevigata extract as an eco-friendly corrosion inhibitor for copper in acidic medium, *J. Taiwan Inst. Chem. Eng*., 2022, **136**, 104408. doi: 10.1016/j.jtice.2022.104408
88. A. Chaouiki, H. Lgaz, R. Salghi, M. Chafiq, S.L. Gaonkar, K.S. Bhat, H. Oudda, I.H. Ali and I.-M. Chung, Inhibitory effect of a new isoniazid derivative as an effective inhibitor for mild steel corrosion in 1.0 M HCl: combined experimental and computational study, *Res. Chem. Intermed*., 2020, **46**, 2919–2950. doi: 10.1007/s11164-020-04119-6

89. J.P. Hansen and I.R. McDonald, *Theory of simple liquids: with applications to soft matter*, Academic Press, 2013.
90. S.-W. Xie, Z. Liu, G.-C. Han, W. Li, J. Liu and Z. Chen, Molecular dynamics simulation of inhibition mechanism of 3,5-dibromo salicylaldehyde Schiff's base, *Comput. Theor. Chem*., 2015, **1063**, 50–62. doi: 10.1016/j.comptc.2015.04.003

♦ ♦ ♦